
iSCAN: Identifying Causal Mechanism Shifts among Nonlinear Additive Noise Models

Tianyu Chen^{*†} Kevin Bello^{‡§} Bryon Aragam[‡] Pradeep Ravikumar[§]

[†]Department of Statistics and Data Science, University of Texas at Austin

[‡]Booth School of Business, University of Chicago

[§]Machine Learning Department, Carnegie Mellon University

Abstract

Structural causal models (SCMs) are widely used in various disciplines to represent causal relationships among variables in complex systems. Unfortunately, the underlying causal structure is often unknown, and estimating it from data remains a challenging task. In many situations, however, the end goal is to localize the changes (shifts) in the causal mechanisms between related datasets instead of learning the full causal structure of the individual datasets. Some applications include root cause analysis, analyzing gene regulatory network structure changes between healthy and cancerous individuals, or explaining distribution shifts. This paper focuses on identifying the causal mechanism shifts in two or more related datasets over the same set of variables—*without estimating the entire DAG structure of each SCM*. Prior work under this setting assumed linear models with Gaussian noises; instead, in this work we assume that each SCM belongs to the more general class of *nonlinear* additive noise models (ANMs). A key technical contribution of this work is to show that the Jacobian of the score function for the *mixture distribution* allows for the identification of shifts under general non-parametric functional mechanisms. Once the shifted variables are identified, we leverage recent work to estimate the structural differences, if any, for the shifted variables. Experiments on synthetic and real-world data are provided to showcase the applicability of this approach. Code implementing the proposed method is open-source and publicly available at <https://github.com/kevinsbello/iSCAN>.

1 Introduction

Structural causal models (SCMs) are powerful models for representing causal relationships among variables in a complex system [54, 58]. Every SCM has an underlying graphical structure that is generally assumed to be a directed acyclic graph (DAG). Identifying the DAG structure of an SCM is crucial since it enables reasoning about interventions [54]. Nonetheless, in most situations, scientists can only access *observational* or *interventional* data, or both, while the true underlying DAG structure remains *unknown*. As a result, in numerous disciplines such as computational biology [66, 30, 20], epidemiology [64], medicine [61, 62], and econometrics [34, 28, 18], it is critically important to develop methods that can estimate the entire underlying DAG structure based on available data. This task is commonly referred to as causal discovery or structure learning, for which a variety of algorithms have been proposed over the last decades.

Throughout this work, we make the assumption of causal sufficiency (i.e., non-existence of unobserved confounders). Under this condition alone, identifying the underlying DAG structure is not possible in general, and remains worst-case NP-complete [14, 16]. Indeed, prominent methods such as PC [71]

^{*}Work done while at the Department of Statistics at the University of Chicago. Correspondence to kbello@cs.cmu.edu.

and GES [15] additionally require the arguably strong faithfulness assumption [77] to consistently estimate, in large samples, the Markov equivalent class of the underlying DAG. However, these methods are not consistent in high-dimensions unless one additionally assumes sparsity or small maximum-degree of the true DAG [36, 50, 78]. Consequently, the existence of hub nodes, which is a well-known feature in several networks [5, 6, 7], significantly complicates the DAG learning problem.

In many situations, however, the end goal is to *detect shifts (changes) in the causal mechanisms* between two (or more) related SCMs rather than recovering the *entire* underlying DAG structure of each SCM. For example, examining the mechanism changes in the gene regulatory network structure between healthy individuals and those with cancer may provide insights into the genetic factors contributing to the specific cancer; within biological pathways, genes could regulate various target gene groups depending on the cellular environment or the presence of particular disease conditions [32, 60]. In these examples, while the individual networks could be *dense*, the number of mechanism shifts could be *sparse* [69, 74, 55]. Finally, in root cause analysis, the goal is to identify the sources that originated observed changes in a joint distribution; this is precisely the setting we study in this work, where we model the joint distributions via SCMs, as also done in [52, 33].

In more detail, we focus on the problem of identifying mechanism shifts given datasets from two or more environments (SCMs) over the same observables. We assume that each SCM belongs to the class of additive noise models (ANMs) [29], i.e., each variable is defined as a nonlinear function over a subset of the remaining variables plus a random noise (see Section 2 for formal definitions). Importantly, we *do not* make any structural assumptions (e.g., sparsity, small maximum-degree, or bounded tree-width) on the individual DAGs. Even though ANMs are well-known to be identifiable [29, 59], we aim to detect the *local distribution changes* without estimating the full structures individually. See Figure 1 for a toy example of what we aim to estimate. A similar setting to this problem was studied in [82, 23] albeit in the restrictive linear setting. Finally, it is worth noting that even with *complete knowledge of the entire structure of each SCM*, assessing changes in *non-parametric* functions across different groups or environments remains a very challenging problem [see for instance, 44].

Contributions. Motivated by recent developments on causal structure learning of ANMs [65], we propose a two-fold algorithm that (1) Identifies shifted variables (i.e., variables for which their causal mechanism has changed across the environments); and (2) If needed, for each shifted variable, estimates the structural changes among the SCMs. More concretely, we make the following set of contributions:

- To identify shifted variables (Definition 3), we prove that the variance of the diagonal elements of the Hessian matrix associated with the log-density of the *mixture distribution* unveils information to detect distribution shifts in the leaves of the DAGs (see Theorem 1). Due to this result, our algorithm (Algorithm 1) iteratively chooses a particular leaf variable and determines whether or not such variable is shifted. Importantly, this detection step **does not** rely on any structural assumptions on the individual DAGs, and can consistently detect distribution shifts for *non-parametric functionals* under very mild conditions such as second-order differentiability.
- To identify structurally shifted edges (Definition 4), we propose a nonparametric local parents recovery method (Algorithm 2) based on a recent measure of conditional dependence [3]. In addition, based on recent results in [4], we provide a theoretical justification for the asymptotic consistency of Algorithm 2 in Theorem 2. Importantly, since structural changes can only occur on *shifted nodes*, this second step can be conducted much more efficiently when the sparse mechanism shift hypothesis [69] holds, which posits that only a small subset of the causal model’s mechanisms change.
- We empirically demonstrate that our method can outperform existing methods such as DCI, which is tailored for linear models, as well as related methods for estimating unknown intervention targets such as UT-IGSP [72]. See Section 5 and Appendix C for more details. Moreover, in Section 5.2, we provide experiments on an ovarian cancer dataset, thus, showcasing the applicability of our method.

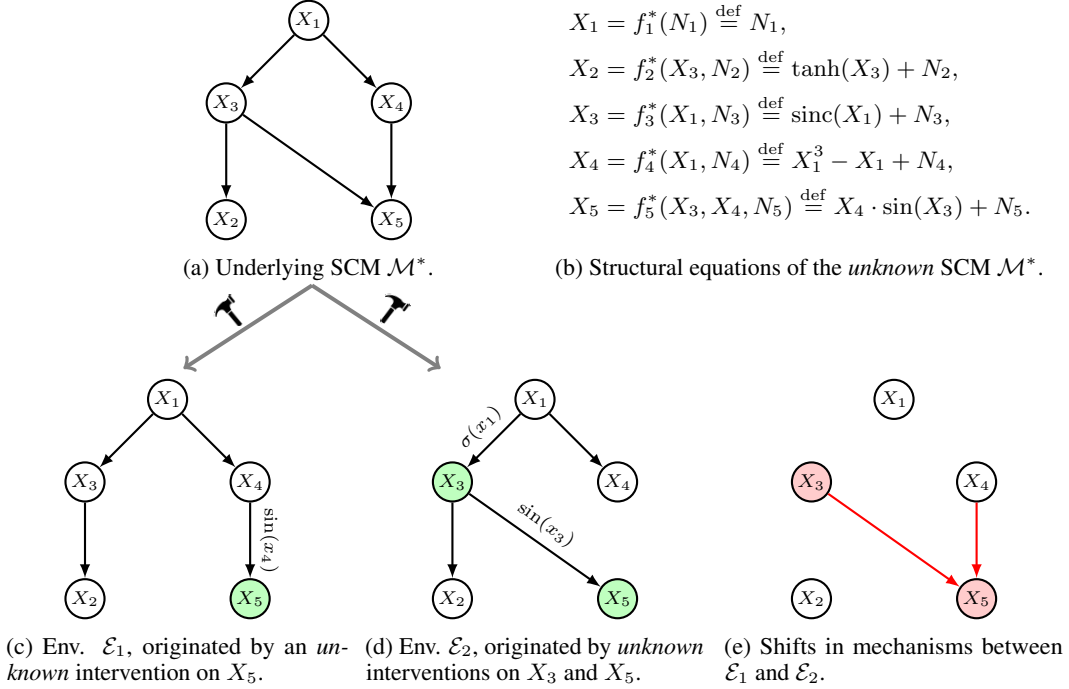


Figure 1: Illustration of two different environments (see Definition 2) in (1c) and (1d), both originated from the underlying SCM in (1a) with structural equations given in (1b). Between the two environments, we observe a change in the causal mechanisms of variables X_3 and X_5 —the red nodes in (1e). Specifically, for X_5 , we observe that its *functional dependence* changed from X_4 in \mathcal{E}_1 to X_3 in \mathcal{E}_2 . For X_3 , its *structural dependence* has not changed between \mathcal{E}_1 and \mathcal{E}_2 , and only its functional changed from $\text{sinc}(X_1)$ in \mathcal{E}_1 to the sigmoid function $\sigma(X_1)$ in \mathcal{E}_2 . Finally, in (1e), the red edges represent the *structural* changes in the mechanisms. The non-existence of an edge from X_1 to X_3 indicates that the structural relation between X_1 and X_3 is invariant.

2 Preliminaries and Background

In this section we introduce notation and formally define the problem setting. We use $[d]$ to denote the set of integers $\{1, \dots, d\}$. Let $G = ([d], E)$ be a DAG with node set $[d]$ and a set of directed edges $E \subset [d] \times [d]$, where any $(i, j) \in E$ indicates and edge from i to j . Also let $X = (X_1, \dots, X_d)$ denote a d -dimensional vector of random variables. An SCM $\mathcal{M} = (X, f, \mathbb{P}_N)$ over d variables is generally defined as a collection of d structural equations of the form:

$$X_j = f_j(\text{PA}_j, N_j), \forall j \in [d], \quad (1)$$

where $\text{PA}_j \subseteq \{X_1, \dots, X_d\} \setminus \{X_j\}$ are the *direct causes* (or parents) of X_j ; $f = \{f_j\}_{j=1}^d$ is a set of *functional mechanisms* $f_j : \mathbb{R}^{|\text{PA}_j|+1} \rightarrow \mathbb{R}$; and \mathbb{P}_N is a joint distribution² over the noise variables N_j , which we assume to be jointly independent³. Moreover, the underlying graph G of an SCM is constructed by drawing directed edges for each $X_k \in \text{PA}_j$ to X_j . We henceforth assume this graph to be acyclic, i.e., a DAG. Finally, every SCM \mathcal{M} defines a unique distribution \mathbb{P}_X over the variables X [Proposition 6.3 in 58], which by the independence of the noise variables (a.k.a. the Markovian assumption), \mathbb{P}_X admits the following factorization:

$$\mathbb{P}(X) = \prod_{j=1}^d \mathbb{P}(X_j | \text{PA}_j), \quad (2)$$

where $\mathbb{P}(X_j | \text{PA}_j)$ is referred as the *causal mechanism* of X_j .

²We will always assume the existence of a density function w.r.t. the Lebesgue measure.

³Note that this implies that there is no hidden confounding.

The model above is often too general due to problems of identifiability. In this work we will consider that the noises are additive.

Definition 1 (Additive noise models (ANMs)). *An additive noise model is an SCM $\mathcal{M} = (X, f, \mathbb{P}_N)$ as in (1), where each structural assignment has the form:*

$$X_j = f_j(\text{PA}_j) + N_j, \forall j \in [d].$$

Depending on the assumptions on f_j and N_j , the underlying DAG of an ANM can be identifiable from observational data. E.g., when f_j is linear and N_j is Gaussian, in general one can only identify the Markov equivalence class (MEC) of the DAG, assuming faithfulness [54]. For linear models, an exception arises when assuming equal error variances [56, 78, 47], or non-Gaussian errors [70]. In addition, when f_j is nonlinear on each component and three times differentiable then the DAG is also identifiable [59, 29]. Very recently, Rolland et al. [65] proved DAG identifiability when f_j is nonlinear on each component and N_j is Gaussian, using information from the score’s Jacobian.

2.1 Data from multiple environments

Throughout this work we assume that we observe a collection of datasets, $\mathcal{D} = \{\mathbf{X}^h\}_{h=1}^H$, from H (possibly different) environments. Each dataset $\mathbf{X}^h = \{X^{h,i}\}_{i=1}^{m_h}$ from environment h contains m_h (possibly non-independent) samples from the joint distribution \mathbb{P}_X^h , i.e., $\mathbf{X}^h \in \mathbb{R}^{m_h \times d}$. We consider that each environment originates from soft interventions⁴ [54] of an *unknown* underlying SCM \mathcal{M}^* with DAG structure G^* and joint distribution $\mathbb{P}^*(X) = \prod_{j=1}^d \mathbb{P}^*(X_j | \text{PA}_j^*)$. Here PA_j^* denotes the parents (direct causes) of X_j in G^* . Then, an environment arises from manipulations or shifts in the causal mechanisms of a *subset* of variables, transforming from $\mathbb{P}^*(X_j | \text{PA}_j^*)$ to $\tilde{\mathbb{P}}(X_j | \tilde{\text{PA}}_j^h)$. Throughout, we will make the common modularity assumption of causal mechanisms [54, 38], which postulates that an intervention on a node X_j only changes the mechanism $\mathbb{P}(X_j | \text{PA}_j)$, while all other mechanisms $\mathbb{P}(X_i | \text{PA}_i)$, for $i \neq j$, remain unchanged.

Definition 2 (Environment). *An environment $\mathcal{E}_h = (X, f^h, \mathbb{P}_N^h)$, with joint distribution \mathbb{P}_X^h and density p_x^h , independently results from an SCM \mathcal{M}^* by intervening on an unknown subset $S^h \subseteq [d]$ of causal mechanisms, that is, we can factorize the joint distribution $\mathbb{P}^h(X)$ as follows:*

$$\mathbb{P}^h(X) = \prod_{j \in [d]} \mathbb{P}^h(X_j | \text{PA}_j^h) = \prod_{j \in S^h} \tilde{\mathbb{P}}^h(X_j | \tilde{\text{PA}}_j^h) \prod_{j \notin S^h} \mathbb{P}^*(X_j | \text{PA}_j^*), \quad (3)$$

where $\tilde{\text{PA}}_j^h$ is a (possibly empty) subset of the underlying causal parents PA_j^* , i.e., $\tilde{\text{PA}}_j^h \subseteq \text{PA}_j^*$; and, $\mathbb{P}^*(X_j | \text{PA}_j^*)$ are the invariant mechanisms.

Remark 1. *In the literature [e.g., 55], it is common to find the assumption that in a soft intervention the direct causes remain invariant, i.e., $\tilde{\text{PA}}_j^h = \text{PA}_j^*$ for all $j \in S^h, h \in [H]$. In this work we consider a more general setting where none, some, or all of the direct causes of an intervened node are removed, i.e., $\tilde{\text{PA}}_j^h \subseteq \text{PA}_j^*$ for all $j \in S^h, h \in [H]$.*

We next define shifted nodes (variables).

Definition 3 (Shifted node). *Given H environments $\{\mathcal{E}_h = (X, f^h, \mathbb{P}_N^h)\}_{h=1}^H$ originated from an ANM \mathcal{M}^* , a node j is called a shifted node if there exists $h, h' \in [H]$ such that:*

$$\mathbb{P}^h(X_j | \text{PA}_j^h) \neq \mathbb{P}^{h'}(X_j | \text{PA}_j^{h'}).$$

To conclude this section, we formally define the problem setting.

Problem setting. Given H datasets $\{\mathbf{X}^h\}_{h=1}^H$, where $\mathbf{X}^h \sim \mathbb{P}_X^h$ consists of m_h (possibly non-independent) samples from the environment distribution \mathbb{P}_X^h originated from an underlying ANM \mathcal{M}^* , estimate the set of shifted nodes and structural differences.

We note that [82, 23] have study the problem setting above for $H = 2$, assuming *linear functions* f_j^h , and Gaussian noises N_j^h . In this work, we consider a more challenging setting where f_j^h are nonparametric functions (see Section 3 for more details).

⁴These types of interventions are more realistic in practice than “hard” or perfect interventions. However, note that we allow a soft intervention on a variable to remove some or all of its causes, where the latter is also known as an stochastic hard intervention.

2.2 Related Work

First we mention works most closely related to ours. The problem of learning the difference between *undirected* graphs has received much more attention than the directed case. E.g., [88, 46, 85, 19] develop algorithms for estimating the difference between Markov random fields and Ising models. See [87] for recent developments in this direction. In the directed setting, [82, 23] propose methods for directly estimating the difference of linear ANMs with Gaussian noise. More recently, [67] studied the setting where a dataset is generated from a mixture of SCMs, and their method is capable of detecting conditional distributions changes; however, due to the unknown membership of each sample, it is difficult to test for structural and functional changes. Moreover, in contrast to ours, all the aforementioned work on the directed setting rely on some form of faithfulness assumption.

Causal discovery from a single environment. One way to identify mechanism shifts (albeit inefficient) would be to estimate the individual DAGs for each environment and then test for structural differences across the different environments. A few classical and recent methods for learning DAGs from a single dataset include: Constraint-based algorithms such as PC and FCI [71]; in score-based methods, we have greedy approaches such as GES [16], likelihood-based methods [56, 47, 59, 2, 1, 29], and continuous-constrained learning [89, 51, 39, 8]. Order-based methods [75, 41, 24, 65, 48], methods that test for asymmetries [70, 12], and hybrid methods [50, 76]. Finally, note that even if we *perfectly estimate each individual DAG* (assuming identifiable models such as ANMs), applying these methods would only identify *structural* changes. That is, for variables that have the same parents across all the environments, we would require an additional step to identify *distributional* changes.

Testing functional changes in multiple datasets. Given the parents of a variable X_j , one could leverage prior work [44, 25, 9, 26] on detecting heterogeneous functional relationships. However, we highlight some important limitations. Several methods such as [25, 9, 26] only work for one dimensional functionals and assume that the datasets share the exact same design matrix. Although [44] relaxes this assumption and extends the method to multivariate cases, the authors assume that the covariates (i.e., PA_j^h) are sampled from the *same distribution* across the environments, which is a strong assumption in our context since ancestors of X_j could have experienced mechanism shifts. Finally, methods such as [53] and [11], although nonparametric, need knowledge about the parent set PA_j for each variable, and they assume that PA_j is same across different environments.

Causal discovery from heterogeneous data. Another well-studied problem is to learn the underlying DAG of the SCM \mathcal{M}^* that originated the different environments. Under this setting, [83] provided a characterization of the \mathcal{I} -MEC, a subset of the Markov equivalence class. [55] provided DAG-identifiability results by leveraging sparse mechanism shifts and relies on identifying such shifts, which this work aims to solve. [10] developed an estimator considering unknown intervention targets. [79] primarily focuses on linear SEM and does not adapt well to nonlinear scenarios. Also assuming linear models, [22, 21] applied ideas from linear invariant causal prediction [ICP, 57] and ICM to identify the causal DAG. [72] proposes a nonparametric method that can identify the intervention targets; however, this method relies on nonparametric CI tests, which can be time-consuming and sample inefficient. [49] introduced the joint causal inference (JCI) framework, which can also estimate intervention nodes. However, this method relies on an assumption that the intervention variables are fully connected, a condition that is unlikely to hold in practice. [31] introduced a two-stage approach that removes functional restrictions. First, they used the PC algorithm using all available data to identify the MEC. Then, the second step aims to orient the remaining edges based on a novel measure of mechanism dependence. Finally, we note that a common assumption in the aforementioned methods is the knowledge of which dataset corresponds to the observational distribution; without such information, their assumptions on the type of interventions would not hold true. In contrast, our method does not require knowledge of the observational distribution.

3 Identifying Causal Mechanism Shifts via Score Matching

In this section, we propose iSCAN (*identifying Shifts in Causal Additive Noise models*), a method for detecting shifted nodes (Definition 3) based only on information from the Jacobian of the score of the data distribution⁵.

⁵In this work, the score of a pdf $p(x)$ means $\nabla \log p(x)$

Let \mathbf{X} be the row concatenation of all the datasets \mathbf{X}^h , i.e., $\mathbf{X} = [(\mathbf{X}^1)^\top | \dots | (\mathbf{X}^H)^\top]^\top \in \mathbb{R}^{m \times d}$, where $m = \sum_{h=1}^H m_h$. The pooled data \mathbf{X} can be interpreted as a mixture of data from the H different environments. To account for this mixture, we introduce the probability mass w_h , which represents the probability that an observation belongs to environment h , i.e., $\sum_{h=1}^H w_h = 1$. Let $\mathbb{Q}(X)$ denote the distribution of the mixture data with density function $q(x)$, i.e., $q(x) = \sum_{h=1}^H w_h p^h(x)$.

In the sequel, we use $s^h(x) \equiv \nabla \log p^h(x)$ to denote the score function of the joint distribution of environment h with density $p^h(x)$. Also, we let $s(x) \equiv \nabla \log q(x)$ to denote the score function of the mixture distribution with density $q(x)$. We will make the following assumptions on f_j^h and N_j^h .

Assumption A. For all $h \in [H], j \in [d]$, the functional mechanisms $f_j^h(\text{PA}_j^h)$ are assumed to be non-linear in every component.

Assumption B. For all $j \in [d], h \in [H]$, the pdf of the real-valued noise N_j^h denoted by $p_{N_j^h}^h$ satisfies $\frac{\partial^2}{(\partial n_j^h)^2} \log p_{N_j^h}^h(n_j^h) = c_j^h$ where c_j^h is a non-zero constant. Moreover, $\mathbb{E}[N_j^h] = 0$.

For an ANM, Rolland et al. [65] showed that under Assumption A and assuming zero-mean Gaussian noises (which satisfies Assumption B), the diagonal of the Jacobian of the score function reveals the leaves of the underlying DAG. We next instantiate their result in our context.

Proposition 1 (Lemma 1 in [65, 68]). For an environment \mathcal{E}_h with underlying DAG G^h and pdf $p^h(x)$, let $s^h(x) = \nabla \log p^h(x)$ be the associated score function. Then, under Assumptions A and B, for all $j \in [d]$, we have:

$$\text{Node } j \text{ is a leaf in } G^h \iff \text{Var}_X \left[\frac{\partial s_j^h(X)}{\partial x_j} \right] = 0.$$

Motivated by the ideas of leaf-identifiability from the score's Jacobian in a single ANM, we next show that the score's Jacobian of the mixture distribution can help reveal mechanism shifts among the different environments.

Theorem 1. For all $h \in [H]$, let G^h and $p^h(x)$ denote the underlying DAG structure and pdf of environment \mathcal{E}_h , respectively, and let $q(x)$ be the pdf of the mixture distribution of the H environments such that $q(x) = \sum_{h=1}^H w_h p^h(x)$. Also, let $s(x) = \nabla \log q(x)$ be the associated score function. Then, under Assumptions A, and B, we have:

- (i) If j is a leaf in all DAGs G^h , then j is a shifted node if and only if $\text{Var}_X \left[\frac{\partial s_j(X)}{\partial x_j} \right] > 0$.
- (ii) If j is not a leaf in at least one DAG G^h , then $\text{Var}_X \left[\frac{\partial s_j(X)}{\partial x_j} \right] > 0$.

Theorem 1 along with Proposition 1 suggests a way to identify shifted nodes. Namely, to use Proposition 1 to identify a common leaf, and then use Theorem 1 to test if such a leaf is a shifted node or not. We then proceed to remove the leaf and repeat the process. See Algorithm 1. Note that due to the fact that each environment is a result of an intervention (Definition 2) on an underlying ANM \mathcal{M}^* , it follows that the leaves in G^* will remain leaves in each DAG G^h .

Algorithm 1 iSCAN—Identifying Shifts in Causal Additive Noise models.

Input: Datasets $\mathbf{X}^1, \dots, \mathbf{X}^H$.

Output: Shifted variables set \widehat{S} , and topological sort $\widehat{\pi}$.

- 1: Initialize $\widehat{S} = \{\}$, $\widehat{\pi} = ()$, $\mathcal{N} = \{1, \dots, d\}$
 - 2: Set $\mathbf{X} = [(\mathbf{X}^1)^\top | \dots | (\mathbf{X}^H)^\top]^\top \in \mathbb{R}^{m \times d}$.
 - 3: **while** $\mathcal{N} \neq \emptyset$ **do**
 - 4: $\forall h \in [H], \text{Var}^h \leftarrow \text{Var}_{\mathbf{X}^h} [\text{diag}(\nabla^2 \log p^h(x))]$.
 - 5: $\text{Var} \leftarrow \text{Var}_{\mathbf{X}} [\text{diag}(\nabla^2 \log q(x))]$
 - 6: $L \leftarrow \bigcap_{h \in [H]} \{j \mid \text{Var}_j^h = 0, j \in [d]\}$. ▷ Identify leaves.
 - 7: $\widehat{S} \leftarrow \widehat{S} \cup \{j \mid \text{Var}_j \neq 0, j \in L\}$ ▷ Identify shifted nodes.
 - 8: $\mathcal{N} \leftarrow \mathcal{N} - \{L\}$
 - 9: $\forall l \in L$, remove the l -th column of $\mathbf{X}^h, \forall h \in [H]$, and \mathbf{X} .
 - 10: $\widehat{\pi} \leftarrow (L, \widehat{\pi})$.
-

Remark 2. See Appendix A for a practical implementation of Alg. 1. Finally, note that Alg. 1 also estimates a valid topological sort for the different environments by leveraging Proposition 1.

3.1 Score’s Jacobian estimation

Since the procedure to estimate $\text{Var}_q[\frac{\partial s_j(x)}{\partial x_j}]$ is similar for estimating $\text{Var}_{p^h}[\frac{\partial s_j^h(x)}{\partial x_j}]$ for each $h \in [H]$, in this section we discuss the estimation for $\text{Var}_q[\frac{\partial s_j(x)}{\partial x_j}]$, which involves computing the diagonal of the Hessian of $\log q(x)$. To estimate this quantity, we adopt a similar approach to the method in [45, 65]. First, we estimate the first-order derivative of $\log q(x)$ by Stein’s identity [73]:

$$\mathbb{E}_q \left[\mathbf{h}(x) \nabla \log q(x)^\top + \nabla \mathbf{h}(x) \right] = 0, \quad (4)$$

where $\mathbf{h} : \mathbb{R}^d \rightarrow \mathbb{R}^{d'}$ is any test function such that $\lim_{x \rightarrow \infty} \mathbf{h}(x)q(x) = 0$. Once we have estimated $\nabla \log q(x)$, we can proceed to estimate the Hessian’s diagonal by using second-order Stein’s identity:

$$\mathbb{E}_q[\mathbf{h}(x) \text{diag}(\nabla^2 \log q(x))^\top] = \mathbb{E}_q[\nabla_{\text{diag}}^2 \mathbf{h}(x) - \mathbf{h}(x) \text{diag}(\nabla \log q(x) \nabla \log q(x)^\top)] \quad (5)$$

Using eq.(4) and eq.(5), we can estimate the Hessian’s diagonal at each data point. Thus allowing us to obtain an estimate of $\text{Var}_q[\frac{\partial s_j(x)}{\partial x_j}]$. See Appendix A.1 for additional details.

Remark 3 (Consistency of Algorithm 1). *The estimators in eq.(6) and eq.(7), given in Appendix A.1, correspond to Monte Carlo estimators using eq.(4) and (5), respectively, then the error of the estimators tend to zero as the number of samples goes to infinity. See for instance the discussion in Section 3.1 in [45]. We empirically explore the consistency of Algorithm 1 in Figure 2.*

Remark 4 (Computational Complexity). *Since we adopt the kernel-based estimator, SCORE, from [65]. The computational complexity for the estimation of the score’s Jacobian in a single environment is $\mathcal{O}(dm_h^3)$. In Algorithm 1, computation is dominated by the SCORE function applied to the pooled data $\mathbf{X} \in \mathbb{R}^{m \times d}$. Therefore, the overall complexity of Algorithm 1 is $\mathcal{O}(dm^3)$. See Figure 2.*

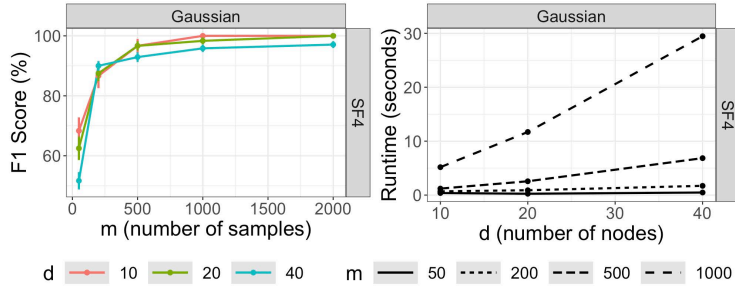


Figure 2: (Left) F1 score of the output of Alg. 1 w.r.t. to the true set of shifted nodes. For different number of nodes, we observe how iSCAN recovers the true set of shifted nodes as the number of samples increases, thus empirically showing its consistency. (Right) Runtime vs number of nodes for different number of samples. We corroborate the linear dependence of the time complexity on d .

4 On Identifying Structural Differences

After estimating the set of shifted nodes \hat{S} through Algorithm 1, it is of high interest to predict which causal relations between a shifted node and its parents have undergone changes across the environments. The meaning of a change in a causal relationship can vary based on the context and the estimation objective. This section primarily centers on structural changes, elaborated further below, while additional discussion about other types of changes is available in Appendix D.

Definition 4 (Structurally shifted edge). *For a given shifted node X_j , an edge $X_i \rightarrow X_j$ is called a structurally shifted edge if $\exists h, h' \in [H]$ such that $X_i \in \text{PA}_j^h$ and $X_i \notin \text{PA}_j^{h'}$.*

In other words, a structurally shifted edge is an edge that exists in one environment but not in another, indicating a change in the underlying structure of the causal mechanism. To detect the structurally shifted edges, we will estimate the parents of each shifted node in \hat{S} for all environments \mathcal{E}_h .

Remark 5. Note that under the sparse mechanism shift hypothesis [69], i.e., $|S| \ll d$, estimating the parents of each shifted node is much more efficient than estimating the entire individual structures.

Kernel regression and variable selection. A potential strategy to estimate structurally shifted edges involves employing the estimated topological order $\hat{\pi}$ obtained from Algorithm 1. If this estimated topological order remains valid across all environments, it can serve as a guide for the nonparametric variable selection process to identify the parents of a shifted node X_j . Specifically, we can regress the shifted node X_j on its predecessors $\widehat{\text{Pre}}(X_j)$ and proceed with a nonparametric variable selection procedure. Here $\widehat{\text{Pre}}(X_j)$ consists of the set of nodes that appear before X_j in the estimated topological order $\hat{\pi}$. To achieve that, there exist various methods under the hypothesis testing framework [42, 17, 63], and bandwidth selection procedures [40]. These methods offer consistency guarantees, but their time complexity might be problematic. Kernel regression, for example, has a time complexity of $\mathcal{O}(m^3)$, and requires an additional bandwidth selection procedure, usually with a time complexity of $\mathcal{O}(m^2)$. Consequently, it becomes imperative to find a more efficient method for identifying parents locally.

Feature ordering by conditional independence (FOCI). An alternative efficient approach for identifying the parents is to leverage the feature ordering method based on conditional independence proposed by Azadkia and Chatterjee [3]. This method provides a measure of conditional dependency between variables with a time complexity of $\mathcal{O}(m \log m)$. By applying this method, we can perform fast variable selection in a nonparametric setting. See Algorithm 4 in Appendix A.3.

Theorem 2 (Consistency of Algorithm 4). *Under Assumption C, given in Appendix B.2, if the estimated topological order $\hat{\pi}$ output from Algorithm 1 is valid for all environments, then the output $\widehat{\text{PA}}_j^h$ of Algorithm 4 is equal to the true parents PA_j^h of node X_j with high probability, for all $h \in [H]$.*

Motivated by Theorem 2, we next present Algorithm 2, a procedure to estimate the structurally shifted edges. Given the consistency of Alg. 1 and Alg. 2, it follows that combining both algorithms will correctly estimate the true set of shifted nodes and structural shifted edges, asymptotically.

Algorithm 2 Identifying structurally shifted edges

Input: Data $\{\mathbf{X}^h\}_{h \in [H]}$, topological order $\hat{\pi}$, shifted nodes \widehat{S}

Output: Structurally shifted edges set \widehat{E}

- 1: Initialize $\widehat{E} = \emptyset$
 - 2: **for** X_j in \widehat{S} **do**
 - 3: **for** h in $[H]$ **do**
 - 4: Estimate $\widehat{\text{PA}}_j^h$ from Alg. 4 (FOCI) with input $\{\widehat{\text{Pre}}(\mathbf{X}_j^h), \mathbf{X}_j^h\}$
 - 5: **if** $\exists X_k, h, h'$ such that $X_k \in \widehat{\text{PA}}_j^h, X_k \notin \widehat{\text{PA}}_j^{h'}$ **then**
 - 6: $\widehat{E} \leftarrow \widehat{E} \cup (X_k, X_j)$
-

5 Experiments

We conducted a comprehensive evaluation of our algorithms. Section 5.1 focuses on assessing the performance of iSCAN (Alg. 1) for identifying shifted variables. In Section 5.2, we apply iSCAN for identifying shifted nodes along with FOCI (Alg. 2) for estimating structural changes, on apoptosis data. Also, in App. C, we provide additional experiments including: (i) Localizing shifted nodes without structural changes (App. C.1), and where the functionals are sampled from Gaussian processes (App. C.1.1); (ii) Localizing shifted nodes and estimating structural changes when the underlying graphs are different; and (iii) Evaluating iSCAN using the elbow method for selecting shifted nodes (see App. C.3 and Remark 6). Code is publicly available at <https://github.com/kevinsbello/iSCAN>.

5.1 Synthetic experiments on shifted nodes

Graph models. We generated random graphs using the Erdős-Rényi (ER) and scale free (SF) models. For a given number of variables d , $\text{ER}k$ and $\text{SF}k$ indicate an average number of edges equal to kd .

Data generation. We first sampled a DAG, G^1 , of d nodes according to either the ER or SF model for env. \mathcal{E}_1 . For env. \mathcal{E}_2 , we initialized its DAG structure from env. \mathcal{E}_1 and produced structural changes by randomly selecting $0.2 \cdot d$ nodes from the non-root nodes. This set of selected nodes S , with cardinality $|S| = 0.2d$, correspond to the set of “shifted nodes”. In env. \mathcal{E}_2 , for each shifted node $X_j \in S$, we uniformly at random deleted at most three of its incoming edges, and use D_j to denote the parents whose edges to X_j were deleted; thus, the DAG G^2 is a subgraph of G^1 . Then, in \mathcal{E}_1 , each X_j was defined as follows:

$$X_j = \sum_{i \in \text{PA}_j^1 \setminus D_j} \sin(X_i^2) + \sum_{i \in D_j} 4 \cos(2X_i^2 - 3X_i) + N_j$$

In \mathcal{E}_2 , each X_j was defined as follows:

$$X_j = \sum_{i \in \text{PA}_j^2} \sin(X_i^2) + N_j$$

Experiment details. For each simulation, we generated 500 data points per environment, i.e., $m_1 = 500, m_2 = 500$ and $m = 1000$. The noise variances were set to 1. We conducted 30 simulations for each combination of graph type (ER or SF), noise type (Gaussian, Gumbel, and Laplace), and number of nodes ($d \in \{10, 20, 30, 50\}$). The running time was recorded by executing the experiments on an Intel Xeon Gold 6248R Processor with 8 cores. For our method, we used $\eta = 0.05$ for eq.(6) and eq.(7), and a threshold $t = 2$ (see Alg. 3).

Evaluation. We compared the performance of iSCAN against several baselines, which include: DCI [82], the approach by [11], CITE [79], KCD [53], SCORE [65], and UT-IGSP [72]. Figure 3 illustrates the results for ER4 and SF4 graphs. We note that iSCAN consistently outperforms other baselines in terms of F1 score across all scenarios. Importantly, note how the performance of some baselines, like DCI, CITE, Budhathoki’s, and SCORE, degrades faster for graphs with hub nodes, a property of SF graphs. In contrast, iSCAN performs similarly, as it is not dependent on structural assumptions on the individual DAGs. Additionally, it is worth noting that our method exhibits faster computational time than KCD, Budhathoki’s, and SCORE, particularly for larger numbers of nodes.

In Appendix C.1, we provide experiments on sparser graphs such as ER2/SF2, and denser graphs such as ER6/SF6. We also include Precision and Recall in all plots in the supplement.

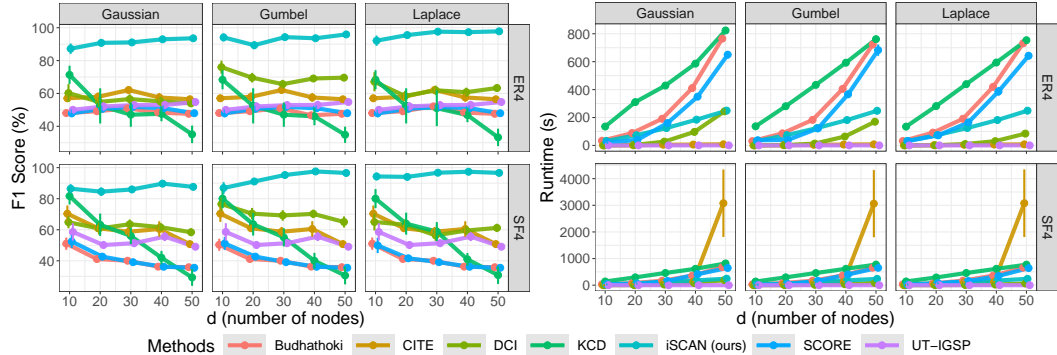
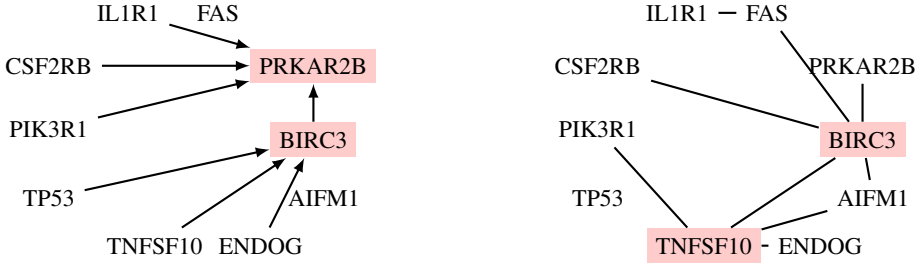


Figure 3: Experiments on ER4 and SF4 graphs. See the experiment details above. The points indicate the average values obtained from these simulations. The error bars depict the standard errors. Our method iSCAN (light blue) consistently outperformed baseline methods in terms of F1 score.

5.2 Experiments on apoptosis data

We conducted an analysis on an ovarian cancer dataset using iSCAN (Algorithm 1) to identify shifted nodes and Algorithm 2 to detect structurally shifted edges (SSEs). This dataset had previously been analyzed using the DPM method [88] in the undirected setting, and the DCI method [82] in the linear setting. By applying our method, we were able to identify the shifted nodes and SSEs in the dataset (see Figure 4a). Our analysis revealed the identification of two hub nodes in the apoptosis

pathway: BIRC3, and PRKAR2B. The identification of BIRC3 as a hub node was consistent with the results obtained by the DPM and DCI methods. Additionally, our analysis also identified PRKAR2B as a hub node, which was consistent with the result obtained by the DCI method. Indeed, BIRC3, in addition to its role in inhibiting TRAIL-induced apoptosis, has been investigated as a potential therapeutic target in cancer treatment including ovarian cancer [35, 81]; whereas PRKAR2B has been identified as an important factor in the progression of ovarian cancer cells. The latter serves as a key regulatory unit involved in the growth and development of cancer cells [84, 13].



(a) The red nodes are the shifted nodes estimated by iSCAN (Alg. 1). The edges are the structurally shifted edges estimated by FOCI (Alg. 2).

(b) Undirected difference network estimated by DPM [88]. The red nodes indicate hub nodes, however, it is not clear which node mechanisms have changed.

Figure 4: Results on apoptosis data.

6 Conclusion

In this work, we showed a novel connection between score matching and identifying causal mechanism shifts among related heterogeneous datasets. This finding opens up a new and promising application for score function estimation techniques.

Our proposed technique consists of three modules. The first module evaluates the Jacobian of the score under the *individual* distributions and the *mixture* distribution. The second module identifies shifted features (variables) using the estimated Jacobians, allowing us to pinpoint the nodes that have undergone a mechanism shift. Finally, the third module aims to estimate structurally shifted edges, a.k.a. the difference DAG, by leveraging the information from the identified shifted nodes and the estimated topological order. *It is important to note that our identifiability result in Theorem 1 is agnostic to the choice of the score estimator.*

The strength of our result lies in its capability to recover the difference DAG in non-linear Additive Noise Models (ANMs) without making any assumptions about the parametric form of the functions or statistical independencies. This makes our method applicable in a wide range of scenarios where non-linear relationships and shifts in mechanisms are present.

6.1 Limitations and future work

While our work demonstrates the applicability of score matching in identifying causal mechanism shifts in the context of nonlinear ANMs, there are several limitations and areas for future exploration:

Extension to other families of SCMs: Currently, our method is primarily focused on ANMs where the noise distribution satisfies Assumption B, e.g., Gaussian distributions. It would be valuable to investigate the application of score matching in identifying causal mechanism shifts in other types of SCMs. Recent literature, such as [48], has extended score matching to additive Models with arbitrary noise for finding the topological order. Expanding our method to accommodate different noise models would enhance its applicability to a wider range of real-world scenarios.

Convergence rate analysis: Although the score matching estimator is asymptotically consistent, the convergence rate remains unknown in general. Understanding the convergence properties of the estimator is crucial for determining the sample efficiency and estimating the required number of samples to control the estimation error within a desired threshold. Further theoretical developments, such as [37], on score matching estimators would provide valuable insights into the performance and sample requirements of iSCAN.

Acknowledgments and Disclosure of Funding

K.B. was supported by NSF under Grant # 2127309 to the Computing Research Association for the CIFellows 2021 Project. B.A. was supported by NSF IIS-1956330, NIH R01GM140467, and the Robert H. Topel Faculty Research Fund at the University of Chicago Booth School of Business. P.R. was supported by ONR via N000141812861, and NSF via IIS-1909816, IIS-1955532, IIS-2211907. We are also grateful for the support of the University of Chicago Research Computing Center for assistance with the calculations carried out in this work.

References

- [1] Aragam, B., Amini, A. and Zhou, Q. [2019], ‘Globally optimal score-based learning of directed acyclic graphs in high-dimensions’, *Advances in Neural Information Processing Systems* **32**.
- [2] Aragam, B. and Zhou, Q. [2015], ‘Concave penalized estimation of sparse Gaussian Bayesian networks’, *The Journal of Machine Learning Research* **16**(1), 2273–2328.
- [3] Azadkia, M. and Chatterjee, S. [2021], ‘A simple measure of conditional dependence’, *The Annals of Statistics* **49**(6), 3070–3102.
- [4] Azadkia, M., Taeb, A. and Bühlmann, P. [2021], ‘A fast non-parametric approach for local causal structure learning’, *arXiv e-prints* pp. arXiv–2111.
- [5] Barabási, A.-L. and Albert, R. [1999], ‘Emergence of scaling in random networks’, *science* **286**(5439), 509–512.
- [6] Barabási, A.-L., Gulbahce, N. and Loscalzo, J. [2011], ‘Network medicine: a network-based approach to human disease’, *Nature reviews genetics* **12**(1), 56–68.
- [7] Barabasi, A.-L. and Oltvai, Z. N. [2004], ‘Network biology: understanding the cell’s functional organization’, *Nature reviews genetics* **5**(2), 101–113.
- [8] Bello, K., Aragam, B. and Ravikumar, P. [2022], ‘Dagma: Learning dags via m-matrices and a log-determinant acyclicity characterization’, *arXiv preprint arXiv:2209.08037*.
- [9] Boente, G. and Pardo-Fernández, J. C. [2022], ‘Robust testing to compare regression curves’, *arXiv preprint arXiv:2205.12065*.
- [10] Brouillard, P., Lachapelle, S., Lacoste, A., Lacoste-Julien, S. and Drouin, A. [2020], ‘Differentiable causal discovery from interventional data’, *Advances in Neural Information Processing Systems* **33**, 21865–21877.
- [11] Budhathoki, K., Janzing, D., Bloebaum, P. and Ng, H. [2021], Why did the distribution change?, in ‘International Conference on Artificial Intelligence and Statistics’, PMLR, pp. 1666–1674.
- [12] Bühlmann, P., Peters, J. and Ernest, J. [2014], ‘Cam: Causal additive models, high-dimensional order search and penalized regression’, *The Annals of Statistics* **42**(6), 2526–2556.
- [13] Chiaradonna, F., Balestrieri, C., Gaglio, D. and Vanoni, M. [2008], ‘Ras and pka pathways in cancer: new insight from transcriptional analysis’, *Frontiers in Bioscience-Landmark* **13**(14), 5257–5278.
- [14] Chickering, D. M. [1996], Learning bayesian networks is np-complete, in ‘Learning from data’, Springer, pp. 121–130.
- [15] Chickering, D. M. [2003], ‘Optimal structure identification with greedy search’, *JMLR* **3**, 507–554.
- [16] Chickering, D. M., Heckerman, D. and Meek, C. [2004], ‘Large-sample learning of Bayesian networks is NP-hard’, *Journal of Machine Learning Research* **5**, 1287–1330.
- [17] Delgado, M. A. and Manteiga, W. G. [2001], ‘Significance testing in nonparametric regression based on the bootstrap’, *The Annals of Statistics* **29**(5), 1469–1507.
- [18] Demiralp, S. and Hoover, K. D. [2003], ‘Searching for the causal structure of a vector autoregression’, *Oxford Bulletin of Economics and statistics* **65**, 745–767.
- [19] Fazayeli, F. and Banerjee, A. [2016], Generalized Direct Change Estimation in Ising Model Structure, in ‘International Conference on Machine Learning’.

- [20] Friedman, N., Linial, M., Nachman, I. and Pe'er, D. [2000], Using bayesian networks to analyze expression data, *in* 'Proceedings of the fourth annual international conference on Computational molecular biology', pp. 127–135.
- [21] Ghassami, A., Kiyavash, N., Huang, B. and Zhang, K. [2018], 'Multi-domain causal structure learning in linear systems', *Advances in neural information processing systems* **31**.
- [22] Ghassami, A., Salehkaleybar, S., Kiyavash, N. and Zhang, K. [2017], 'Learning causal structures using regression invariance', *Advances in Neural Information Processing Systems* **30**.
- [23] Ghoshal, A., Bello, K. and Honorio, J. [2019], 'Direct learning with guarantees of the difference dag between structural equation models', *arXiv preprint arXiv:1906.12024*.
- [24] Ghoshal, A. and Honorio, J. [2018], Learning linear structural equation models in polynomial time and sample complexity, *in* 'Proceedings of the Twenty-First International Conference on Artificial Intelligence and Statistics', Vol. 84 of *Proceedings of Machine Learning Research*, PMLR, pp. 1466–1475.
- [25] Hall, P. and Hart, J. D. [1990], 'Bootstrap test for difference between means in nonparametric regression', *Journal of the American Statistical Association* **85**(412), 1039–1049.
- [26] Hardle, W. and Marron, J. S. [1990], 'Semiparametric comparison of regression curves', *The Annals of Statistics* pp. 63–89.
- [27] Hastie, T. J. [2017], Generalized additive models, *in* 'Statistical models in S', Routledge, pp. 249–307.
- [28] Hoover, K. D., Demiralp, S. and Perez, S. J. [2009], 'Empirical identification of the vector autoregression: The causes and effects of us m2', *The methodology and practice of econometrics: a Festschrift in honour of David F. Hendry* pp. 37–58.
- [29] Hoyer, P., Janzing, D., Mooij, J. M., Peters, J. and Schölkopf, B. [2008], 'Nonlinear causal discovery with additive noise models', *Advances in neural information processing systems* **21**.
- [30] Hu, P., Jiao, R., Jin, L. and Xiong, M. [2018], 'Application of causal inference to genomic analysis: advances in methodology', *Frontiers in Genetics* **9**, 238.
- [31] Huang, B., Zhang, K., Zhang, J., Ramsey, J., Sanchez-Romero, R., Glymour, C. and Schölkopf, B. [2020], 'Causal discovery from heterogeneous/nonstationary data', *The Journal of Machine Learning Research* **21**(1), 3482–3534.
- [32] Hudson, N. J., Reverter, A. and Dalrymple, B. P. [2009], 'A differential wiring analysis of expression data correctly identifies the gene containing the causal mutation', *PLoS computational biology* **5**(5), e1000382.
- [33] Ikram, A., Chakraborty, S., Mitra, S., Saini, S., Bagchi, S. and Kocaoglu, M. [2022], 'Root cause analysis of failures in microservices through causal discovery', *Advances in Neural Information Processing Systems* **35**, 31158–31170.
- [34] Imbens, G. W. [2020], 'Potential outcome and directed acyclic graph approaches to causality: Relevance for empirical practice in economics', *Journal of Economic Literature* **58**(4), 1129–1179.
- [35] Johnstone, R. W., Frew, A. J. and Smyth, M. J. [2008], 'The trail apoptotic pathway in cancer onset, progression and therapy', *Nature Reviews Cancer* **8**(10), 782–798.
- [36] Kalisch, M. and Bühlman, P. [2007], 'Estimating high-dimensional directed acyclic graphs with the pc-algorithm.', *Journal of Machine Learning Research* **8**(3).
- [37] Koehler, F., Heckett, A. and Risteski, A. [2022], 'Statistical efficiency of score matching: The view from isoperimetry', *arXiv preprint arXiv:2210.00726*.
- [38] Koller, D. and Friedman, N. [2009], *Probabilistic graphical models: principles and techniques*, MIT press.
- [39] Lachapelle, S., Brouillard, P., Deleu, T. and Lacoste-Julien, S. [2019], 'Gradient-based neural dag learning', *arXiv preprint arXiv:1906.02226*.
- [40] Lafferty, J. and Wasserman, L. [2008], 'Rodeo: Sparse, greedy nonparametric regression'.
- [41] Larranaga, P., Kuijpers, C. M., Murga, R. H. and Yurramendi, Y. [1996], 'Learning bayesian network structures by searching for the best ordering with genetic algorithms', *IEEE transactions on systems, man, and cybernetics-part A: systems and humans* **26**(4), 487–493.

- [42] Lavergne, P. and Vuong, Q. [2000], ‘Nonparametric significance testing’, *Econometric Theory* **16**(4), 576–601.
- [43] Li, C., Shen, X. and Pan, W. [2023], ‘Nonlinear causal discovery with confounders’, *Journal of the American Statistical Association* pp. 1–10.
- [44] Li, X., Jiang, B. and Liu, J. S. [2021], ‘Kernel-based partial permutation test for detecting heterogeneous functional relationship’, *Journal of the American Statistical Association* pp. 1–19.
- [45] Li, Y. and Turner, R. E. [2017], ‘Gradient estimators for implicit models’, *arXiv preprint arXiv:1705.07107*.
- [46] Liu, S., Suzuki, T., Relator, R., Sese, J., Sugiyama, M., Fukumizu, K. et al. [2017], ‘Support consistency of direct sparse-change learning in markov networks’, *The Annals of Statistics*.
- [47] Loh, P.-L. and Buhlmann, P. [2014], ‘High-Dimensional Learning of Linear Causal Networks via Inverse Covariance Estimation’, *Journal of Machine Learning Research*.
- [48] Montagna, F., Noceti, N., Rosasco, L., Zhang, K. and Locatello, F. [2023], ‘Causal discovery with score matching on additive models with arbitrary noise’, *arXiv:2304.03265*.
- [49] Mooij, J. M., Magliacane, S. and Claassen, T. [2020], ‘Joint causal inference from multiple contexts’, *The Journal of Machine Learning Research* **21**(1), 3919–4026.
- [50] Nandy, P., Hauser, A. and Maathuis, M. H. [2018], ‘High-dimensional consistency in score-based and hybrid structure learning’, *The Annals of Statistics* **46**(6A), 3151–3183.
- [51] Ng, I., Ghassami, A. and Zhang, K. [2020], ‘On the role of sparsity and dag constraints for learning linear dags’, *Advances in Neural Information Processing Systems* **33**, 17943–17954.
- [52] Paleyes, A., Guo, S., Scholkopf, B. and Lawrence, N. D. [2023], Dataflow graphs as complete causal graphs, in ‘2023 IEEE/ACM 2nd International Conference on AI Engineering–Software Engineering for AI (CAIN)’, IEEE, pp. 7–12.
- [53] Park, J., Shalit, U., Schölkopf, B. and Muandet, K. [2021], Conditional distributional treatment effect with kernel conditional mean embeddings and u-statistic regression, in ‘International Conference on Machine Learning’, PMLR, pp. 8401–8412.
- [54] Pearl, J. [2009], *CAUSALITY: Models, Reasoning, and Inference*, 2nd edn, Cambridge University Press.
- [55] Perry, R., Von Kügelgen, J. and Schölkopf, B. [2022], ‘Causal discovery in heterogeneous environments under the sparse mechanism shift hypothesis’, *arXiv preprint arXiv:2206.02013*.
- [56] Peters, J. and Bühlmann, P. [2014], ‘Identifiability of gaussian structural equation models with equal error variances’, *Biometrika* **101**(1), 219–228.
- [57] Peters, J., Bühlmann, P. and Meinshausen, N. [2016], ‘Causal inference by using invariant prediction: identification and confidence intervals’, *Journal of the Royal Statistical Society. Series B (Statistical Methodology)* pp. 947–1012.
- [58] Peters, J., Janzing, D. and Schölkopf, B. [2017], *Elements of causal inference: foundations and learning algorithms*, The MIT Press.
- [59] Peters, J., Mooij, J. M., Janzing, D. and Schölkopf, B. [2014], ‘Causal discovery with continuous additive noise models’.
- [60] Pimanda, J. E., Ottersbach, K., Knezevic, K., Kinston, S., Chan, W. Y., Wilson, N. K., Landry, J.-R., Wood, A. D., Kolb-Kokocinski, A., Green, A. R. et al. [2007], ‘Gata2, flil1, and scl form a recursively wired gene-regulatory circuit during early hematopoietic development’, *Proceedings of the National Academy of Sciences* **104**(45), 17692–17697.
- [61] Plis, S. M., Calhoun, V. D., Weisend, M. P., Eichele, T. and Lane, T. [2010], ‘Meg and fmri fusion for non-linear estimation of neural and bold signal changes’, *Frontiers in neuroinformatics* **4**, 114.
- [62] Plis, S. M., Weisend, M. P., Damaraju, E., Eichele, T., Mayer, A., Clark, V. P., Lane, T. and Calhoun, V. D. [2011], ‘Effective connectivity analysis of fmri and meg data collected under identical paradigms’, *Computers in biology and medicine* **41**(12), 1156–1165.
- [63] Racine, J. [1997], ‘Consistent significance testing for nonparametric regression’, *Journal of Business & Economic Statistics* **15**(3), 369–378.

- [64] Robins, J. M., Hernan, M. A. and Brumback, B. [2000], ‘Marginal structural models and causal inference in epidemiology’, *Epidemiology* pp. 550–560.
- [65] Rolland, P., Cevher, V., Kleindessner, M., Russell, C., Janzing, D., Schölkopf, B. and Locatello, F. [2022], Score matching enables causal discovery of nonlinear additive noise models, in ‘International Conference on Machine Learning’, PMLR, pp. 18741–18753.
- [66] Sachs, K., Perez, O., Pe’er, D., Lauffenburger, D. A. and Nolan, G. P. [2005], ‘Causal protein-signaling networks derived from multiparameter single-cell data’, *Science* **308**(5721), 523–529.
- [67] Saeed, B., Panigrahi, S. and Uhler, C. [2020], Causal structure discovery from distributions arising from mixtures of dags, in ‘International Conference on Machine Learning’, PMLR, pp. 8336–8345.
- [68] Sanchez, P., Liu, X., O’Neil, A. Q. and Tsiftaris, S. A. [2022], ‘Diffusion models for causal discovery via topological ordering’, *arXiv preprint arXiv:2210.06201* .
- [69] Schölkopf, B., Locatello, F., Bauer, S., Ke, N. R., Kalchbrenner, N., Goyal, A. and Bengio, Y. [2021], ‘Toward causal representation learning’, *Proceedings of the IEEE* **109**(5), 612–634.
- [70] Shimizu, S., Hoyer, P. O., Hyvärinen, A., Kerminen, A. and Jordan, M. [2006], ‘A linear non-gaussian acyclic model for causal discovery.’, *Journal of Machine Learning Research* .
- [71] Spirtes, P., Glymour, C. N., Scheines, R. and Heckerman, D. [2000], *Causation, prediction, and search*, MIT press.
- [72] Squires, C., Wang, Y. and Uhler, C. [2020], Permutation-based causal structure learning with unknown intervention targets, in ‘Conference on Uncertainty in Artificial Intelligence’, PMLR, pp. 1039–1048.
- [73] Stein, C. [1972], A bound for the error in the normal approximation to the distribution of a sum of dependent random variables, in ‘Proc. Sixth Berkeley Symp. Math. Stat. Prob.’, pp. 583–602.
- [74] Tanay, A., Regev, A. and Shamir, R. [2005], ‘Conservation and evolvability in regulatory networks: the evolution of ribosomal regulation in yeast’, *Proceedings of the National Academy of Sciences* **102**(20), 7203–7208.
- [75] Teyssier, M. and Koller, D. [2012], ‘Ordering-based search: A simple and effective algorithm for learning bayesian networks’, *arXiv preprint arXiv:1207.1429* .
- [76] Tsamardinos, I., Brown, L. E. and Aliferis, C. F. [2006], ‘The max-min hill-climbing Bayesian network structure learning algorithm’, *Machine Learning* **65**(1), 31–78.
- [77] Uhler, C., Raskutti, G., Bühlmann, P. and Yu, B. [2013], ‘Geometry of the faithfulness assumption in causal inference’, *The Annals of Statistics* pp. 436–463.
- [78] Van de Geer, S. and Bühlmann, P. [2013], ‘ ℓ_0 -penalized maximum likelihood for sparse directed acyclic graphs’, *The Annals of Statistics* **41**(2), 536–567.
- [79] Varici, B., Shanmugam, K., Sattigeri, P. and Tajer, A. [2021], ‘Scalable intervention target estimation in linear models’, *Advances in Neural Information Processing Systems* **34**, 1494–1505.
- [80] Voorman, A., Shojaie, A. and Witten, D. [2014], ‘Graph estimation with joint additive models’, *Biometrika* **101**(1), 85–101.
- [81] Vucic, D. and Fairbrother, W. J. [2007], ‘The inhibitor of apoptosis proteins as therapeutic targets in cancer’, *Clinical cancer research* **13**(20), 5995–6000.
- [82] Wang, Y., Squires, C., Belyaeva, A. and Uhler, C. [2018], ‘Direct estimation of differences in causal graphs’, *Advances in neural information processing systems* **31**.
- [83] Yang, K., Katcoff, A. and Uhler, C. [2018], Characterizing and learning equivalence classes of causal dags under interventions, in ‘International Conference on Machine Learning’, PMLR, pp. 5541–5550.
- [84] Yoon, H., Jang, H., Kim, E.-Y., Moon, S., Lee, S., Cho, M., Cho, H. J., Ko, J. J., Chang, E. M., Lee, K.-A. et al. [2018], ‘Knockdown of prkar2b results in the failure of oocyte maturation’, *Cellular Physiology and Biochemistry* **45**(5), 2009–2020.
- [85] Yuan, H., Xi, R., Chen, C. and Deng, M. [2017], ‘Differential network analysis via lasso penalized D-trace loss’, *Biometrika* .

- [86] Zhang, K., Peters, J., Janzing, D. and Schölkopf, B. [2012], ‘Kernel-based conditional independence test and application in causal discovery’, *arXiv preprint arXiv:1202.3775* .
- [87] Zhao, B., Wang, Y. S. and Kolar, M. [2020], ‘Fudge: Functional differential graph estimation with fully and discretely observed curves’, *arXiv preprint arXiv:2003.05402* .
- [88] Zhao, S. D., Cai, T. T. and Li, H. [2014], ‘Direct estimation of differential networks’, *Biometrika* **101**(2), 253–268.
- [89] Zheng, X., Aragam, B., Ravikumar, P. K. and Xing, E. P. [2018], ‘Dags with no tears: Continuous optimization for structure learning’, *NeurIPS* .

SUPPLEMENTARY MATERIAL
iSCAN: Identifying Causal Mechanism Shifts among Nonlinear Additive Noise Models

A Practical Implementation

In this section, we present a more practical version of Alg. 1 that considers estimation errors, see Alg. 3. First, we provide more details of the score’s Jacobian estimation.

A.1 Practical Version of SCORE

Let $\mathbf{X} = \{x^1, \dots, x^m\}$ be a dataset of m possibly non-independent but identically distributed samples. From Li and Turner [45], we next present the estimator for the point-wise first-order partial derivative, corresponding to eq.(4):

$$\hat{\mathbf{G}} = -(\mathbf{K} + \eta \mathbf{I})^{-1} \langle \nabla, \mathbf{K} \rangle \quad (6)$$

where $\mathbf{H} = (h(x^1), \dots, h(x^m)) \in \mathbb{R}^{d \times m}$, $\overline{\nabla \mathbf{h}} = \frac{1}{m} \sum_{k=1}^m \nabla \mathbf{h}(x^k)$, $\mathbf{K} = \mathbf{H}^\top \mathbf{H}$, $K_{ij} = \kappa(x^i, x^j) = \mathbf{h}(x^i)^\top \mathbf{h}(x^j)$, $\langle \nabla, \mathbf{K} \rangle = m \mathbf{H}^\top \overline{\nabla \mathbf{h}}$, $\langle \nabla, \mathbf{K} \rangle_{ij} = \sum_{k=1}^m \nabla_{x_j^k} \kappa(x^i, x^j)$, and $\eta \geq 0$ is a regularization parameter. Here $\hat{\mathbf{G}}$ is used to approximate $\mathbf{G} \equiv (\nabla \log p(x^1), \dots, \nabla \log p(x^m))^\top \in \mathbb{R}^{m \times d}$.

From [65], we now present the estimator for the diagonal elements of the score’s Jacobian at the sample points, i.e. $\mathbf{J} \equiv (\text{diag}(\nabla^2 \log p(x^1)), \dots, (\text{diag}(\nabla^2 \log p(x^m)))^\top \in \mathbb{R}^{m \times d}$, the estimator of \mathbf{J} is:

$$\hat{\mathbf{J}} = -\text{diag}(\hat{\mathbf{G}} \hat{\mathbf{G}}^\top) + (\mathbf{K} + \eta \mathbf{I})^{-1} \langle \nabla_{\text{diag}}^2, \mathbf{K} \rangle \quad (7)$$

where $\mathbf{H} = (h(x^1), \dots, h(x^m)) \in \mathbb{R}^{d \times m}$, $\overline{\nabla_{\text{diag}}^2 \mathbf{h}} = \frac{1}{m} \sum_{k=1}^m \nabla_{\text{diag}}^2 \mathbf{h}(x^k)$, $(\nabla_{\text{diag}}^2 \mathbf{h}(x))_{ij} = \frac{\partial^2 h_i(x)}{\partial x_j^2}$, $\mathbf{K} = \mathbf{H}^\top \mathbf{H}$, $K_{ij} = \kappa(x^i, x^j) = \mathbf{h}(x^i)^\top \mathbf{h}(x^j)$, $\langle \nabla_{\text{diag}}^2, \mathbf{K} \rangle = m \mathbf{H}^\top \overline{\nabla_{\text{diag}}^2 \mathbf{h}}$, $\langle \nabla_{\text{diag}}^2, \mathbf{K} \rangle_{ij} = \sum_{k=1}^m \frac{\partial^2 \kappa(x^i, x^k)}{(\partial x_j^k)^2}$, and $\eta \geq 0$ is a regularization parameter.

In the sequel, we use $\text{SCORE}(\mathbf{X})$ to denote the procedure to compute the sample variance for the estimator of the diagonal of the score’s Jacobian via eq.(7).

A.2 Practical Version of Algorithm 1

Let $\widehat{\text{Var}}^h$ be a d -dimensional vector, where d is the number of nodes. We introduce a d -dimensional vector rank^h , which represents the index of each element in $\widehat{\text{Var}}^h$ after a non-decreasing sorting. For example, if $\widehat{\text{Var}}^h = (5.2, 3.1, 4.5, 1.6)$, then $\text{rank}^h = (3, 1, 2, 0)$. Furthermore, we define a d -dimensional vector rank as the element-wise summation of rank^h over all $h \in [H]$. In other words, rank is calculated as $\text{rank} = \sum_{h \in [H]} \text{rank}^h$.

Recall that in Section 3.1 we remarked that we leverage the SCORE approach from Rolland et al. [65] for estimating $\text{diag}(\nabla^2 \log p(x))$ at each data point. Recall also that our identifiability result (Theorem 1) depends on determining whether a leaf node has variance $\text{Var}_q(\frac{\partial s_j(x)}{\partial x_j}) = 0$. In practice, it is unrealistic to simply test for the equality $\text{Var}_L = 0$ since Var_L carries out errors due to finite samples. Instead, we define the following statistic for each estimated leaf node L (Line 10 in Algorithm 3):

$$\text{stats}_L = \frac{\text{Var}_L}{\min_h \text{Var}_L^h + \epsilon}. \quad (8)$$

Algorithm 3 Practical version of Algorithm 1

Input: Datasets $\mathbf{X}^1, \dots, \mathbf{X}^H$, threshold t

Output: Shifted variables set \widehat{S} , and topological sort $\widehat{\pi}$.

- 1: Initialize $\widehat{S} = \emptyset, \widehat{\pi} = ()$, $\mathcal{N} = \{1, \dots, d\}$
 - 2: $\text{stats} \leftarrow (0, \dots, 0) \in \mathbb{R}^d$
 - 3: Set $\mathbf{X} = [(\mathbf{X}^1)^\top \mid \dots \mid (\mathbf{X}^H)^\top]^\top \in \mathbb{R}^{m \times d}$.
 - 4: **while** $\mathcal{N} \neq \emptyset$ **do**
 - 5: $\forall h \in [H], \widehat{\text{Var}}^h \leftarrow \text{SCORE}(\mathbf{X}^h)$. ▷ Estimate $\text{Var}_{\mathbf{X}^h} [\text{diag}(\nabla^2 \log p^h(x))]$.
 - 6: $\forall h \in [H], \text{rank}^h \leftarrow \text{argsort}(\widehat{\text{Var}}^h)$.
 - 7: $\text{rank} \leftarrow \sum_{h \in [H]} \text{rank}^h$
 - 8: $\widehat{L} \leftarrow \arg \min_j \text{rank}_j$ ▷ Estimate a leaf node
 - 9: $\widehat{\text{Var}} \leftarrow \text{SCORE}(\mathbf{X})$ ▷ Estimate $\text{Var}_{\mathbf{X}} [\text{diag}(\nabla^2 \log q(x))]$.
 - 10: $\text{stats}_L = \frac{\widehat{\text{Var}}_L}{\min_h \widehat{\text{Var}}_L^h}$
 - 11: $\mathcal{N} \leftarrow \mathcal{N} - \{L\}$
 - 12: Remove the \widehat{L} -th column of $\mathbf{X}^h, \forall h \in [H]$, and \mathbf{X} .
 - 13: $\widehat{\pi} \leftarrow (\widehat{L}, \widehat{\pi})$.
 - 14: $\widehat{S} = \{j \mid \text{stats}_j > t, \forall j \in [d]\}$
-

The intuition behind this ratio is that if the leaf node L is a *shifted node* then we can expect $\frac{\widehat{\text{Var}}_L}{\min_h \widehat{\text{Var}}_L^h}$ to be large since $\text{Var}_L > 0$ (by Theorem 1), and $\text{Var}_L^h \approx 0$ (by Proposition 1). On the other hand, if the leaf node L is **not** a shifted node then we can expect $\frac{\widehat{\text{Var}}_L}{\min_h \widehat{\text{Var}}_L^h}$ to be small. This is due to the fact that, given a consistent estimator, Var_L would converge towards 0 (by Theorem 1) at a faster rate than Var_L^h since we utilize a larger amount of data for estimating Var_L . Finally, ϵ in the denominator is a very small value, e.g. 10^{-9} , and acts as a safeguard against encountering a division by zero⁶.

Then, given the statistic in eq.(8), we can set a threshold t and define the set of shifted nodes S by all the nodes j such that $\text{stats}_j > t$ (Line 14 in Algorithm 3).

Remark 6 (The elbow strategy). *Alternatively, we can employ an adaptive approach to identify the set of shifted nodes by sorting stats in non-increasing order, and look for the “elbow” point. For example, Figure 5 illustrates the variance ratio in (8) for each node sorted in non-increasing order. In this case, node index 5 corresponds to the elbow point, allowing us to estimate nodes 5 and 8 as shifted nodes. Identifying the elbow point has the advantage to detect shifted nodes without relying on a fixed threshold.*

A.3 Algorithm details for FOCI

Algorithm 4 Feature ordering by conditional independence (FOCI)

Input: Data $\widehat{\text{Pre}}(\mathbf{X}_j^h), \mathbf{X}_j^h$

Output: Estimated parents of $X_j, \widehat{\text{PA}}_j^h$

- 1: $P \leftarrow \emptyset$
 - 2: Let $T_m(i, j, P) \equiv T_m(\mathbf{X}_j^h, \mathbf{X}_i^h \mid \mathbf{X}_P^h)$ ▷ T_m is the estimator in Azadkia and Chatterjee [3].
 - 3: **while** $\max_{X_i \notin P, X_i \in \widehat{\text{Pre}}(X_j)} T_m(i, j, P) > 0$ **do**
 - 4: $P \leftarrow P \cup \left\{ \arg \max_{X_i \notin P, X_i \in \widehat{\text{Pre}}(X_j)} T_m(i, j, P) \right\}$
 - 5: $\widehat{\text{PA}}_j^h \leftarrow P$
-

⁶In practice, one could omit ϵ from the denominator as it is unusual to obtain $\min_h \text{Var}_L^h = 0$ from finite samples and computational precision.

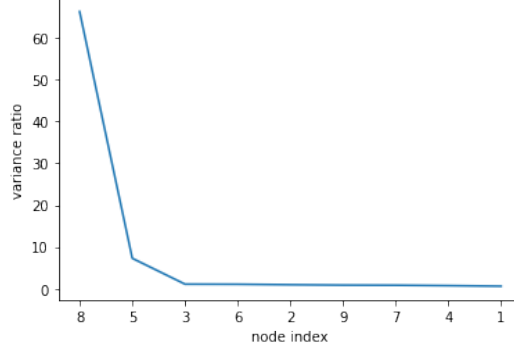


Figure 5: Statistic in eq.(8) for each node sorted in non-increasing order. In this case, node index 5 corresponds to the *elbow point*, allowing us to estimate nodes 5 and 8 as shifted nodes.

B Detailed Proofs

B.1 Proof of Theorem 1

To prove Theorem 1 we will make use of the following lemmas.

Lemma 1. Let $\{a_h\}_{h=1}^H$ and $\{b_h\}_{h=1}^H$ be two sequences of real numbers, where $a_h > 0, \forall h$. Then we have:

$$\left(\sum_{h=1}^H a_h b_h^2 \right) \left(\sum_{h=1}^H a_h \right) - \left(\sum_{h=1}^H a_h b_h \right)^2 \geq 0,$$

with equality if and only if $b_i = b_j, \forall j \neq i \in [H]$.

Proof. We can invoke the Cauchy–Schwarz inequality with vectors $\mathbf{u} = (\sqrt{a_1}, \dots, \sqrt{a_H})$, and $\mathbf{v} = (b_1\sqrt{a_1}, \dots, b_H\sqrt{a_H})$, then we have:

$$(\mathbf{u}^\top \mathbf{v})^2 \leq \|\mathbf{u}\|_2^2 \|\mathbf{v}\|_2^2,$$

which proves the inequality. The equality holds if and only if \mathbf{u} and \mathbf{v} are linearly dependent, i.e., when $b_i = b_j$ for all $i \neq j \in [H]$. \square

Lemma 2. For any j , if $\mathbb{P}^h(X_j | \text{PA}_j^h) = \mathbb{P}^{h'}(X_j | \text{PA}_j^{h'})$, then $c_j^h = c_j^{h'}$.

Proof. Denote the associated density of $\mathbb{P}^h(X_j | \text{PA}_j^h)$ when $X_j = x_j$ as $p_{N_j}^h(x_j - f_j^h(\text{PA}_j^h))$ and let $u = x_j - f_j^h(\text{PA}_j^h)$

$$\begin{aligned} & \frac{\partial^2}{\partial(x_j)^2} \log p_{N_j}^h(x_j - f_j^h(\text{PA}_j^h)) \\ &= \frac{\partial \log p_{N_j}^h(u)}{\partial u} \frac{\partial^2 u}{\partial(x_j)^2} + \frac{\partial^2 \log p_{N_j}^h(u)}{\partial u^2} \left(\frac{\partial u}{\partial x_j} \right)^2 \\ &= 0 + c_j^h = c_j^h \end{aligned}$$

where we use the fact that $\frac{\partial u}{\partial x_j} = 1, \frac{\partial^2 u}{\partial(x_j)^2} = 0$. Then it immediate follows that if $\mathbb{P}^h(X_j | \text{PA}_j^h) = \mathbb{P}^{h'}(X_j | \text{PA}_j^{h'})$, then $c_j^h = c_j^{h'}$ \square

Lemma 3. For any j , under Assumption B, $\frac{\partial}{\partial x_j} \log p_{N_j}^h(x_j - f_j^h(\text{PA}_j^h)) = \frac{\partial}{\partial x_j} \log p_{N_j}^{h'}(x_j - f_j^{h'}(\text{PA}_j^{h'}))$ if and only if $\mathbb{P}^h(X_j | \text{PA}_j^h) = \mathbb{P}^{h'}(X_j | \text{PA}_j^{h'})$, where p^h and $p^{h'}$ are the probability density functions corresponding to the probability measures \mathbb{P}^h and $\mathbb{P}^{h'}$ when $X_j = x_j$.

Proof. Denote the associated density of $\mathbb{P}^h(X_j | \text{PA}_j^h)$ when $X_j = x_j$ as $p_{N_j}^h(x_j - f_j^h(\text{PA}_j^h))$, we proceed as follows:

$$\begin{aligned}
& \frac{\partial}{\partial x_j} \log p_{N_j}^h(x_j - f_j^h(\text{PA}_j^h)) = \frac{\partial}{\partial x_j} \log p_{N_j}^{h'}(x_j - f_j^{h'}(\text{PA}_j^{h'})) \\
\iff & \log p_{N_j}^h(x_j - f_j^h(\text{PA}_j^h)) = \log p_{N_j}^{h'}(x_j - f_j^{h'}(\text{PA}_j^{h'})) + \text{const} \\
\iff & p_{N_j}^h(x_j - f_j^h(\text{PA}_j^h)) = p_{N_j}^{h'}(x_j - f_j^{h'}(\text{PA}_j^{h'})) \cdot e^{\text{const}} \\
& \Rightarrow \int_{\mathbb{R}} p_{N_j}^h(x_j - f_j^h(\text{PA}_j^h)) dx_j = e^{\text{const}} \cdot \int_{\mathbb{R}} p_{N_j}^{h'}(x_j - f_j^{h'}(\text{PA}_j^{h'})) dx_j \\
& \Rightarrow \int_{\mathbb{R}} p_{N_j}^h(x_j - f_j^h(\text{PA}_j^h)) d(x_j - f_j^h(\text{PA}_j^h)) = e^{\text{const}} \cdot \int_{\mathbb{R}} p_{N_j}^{h'}(x_j - f_j^{h'}(\text{PA}_j^{h'})) d(x_j - f_j^{h'}(\text{PA}_j^{h'})) \\
& \Rightarrow 1 = 1 \cdot e^{\text{const}} \\
& \Rightarrow \text{const} = 0
\end{aligned}$$

Here, const is a constant that is independent of x_j . Integrating both sides with respect to x_j and using the fact that $\int p^h(x) dx = 1$, we conclude that $\text{const} = 0$. Hence, we can establish the following:

$$\begin{aligned}
& \frac{\partial}{\partial x_j} \log p_{N_j}^h(x_j - f_j^h(\text{PA}_j^h)) = \frac{\partial}{\partial x_j} \log p_{N_j}^{h'}(x_j - f_j^{h'}(\text{PA}_j^{h'})) \\
\iff & p_{N_j}^h(x_j - f_j^h(\text{PA}_j^h)) = p_{N_j}^{h'}(x_j - f_j^{h'}(\text{PA}_j^{h'})) \\
\iff & \mathbb{P}^h(X_j | \text{PA}_j^h) = \mathbb{P}^{h'}(X_j | \text{PA}_j^{h'})
\end{aligned}$$

□

Proof of Theorem 1. Let us first expand the log density of the mixture distribution:

$$\log q(x) = \log \left(\sum_{h=1}^H w_h p^h(x) \right)$$

Then, recall that $s(x) = \nabla \log q(x)$, the j -entry reads:

$$\begin{aligned}
s_j(x) &= \sum_{h=1}^H \frac{w_h p^h(x)}{\sum_{k=1}^H w_k p^k(x)} \left[\frac{\partial}{\partial x_j} \log p^h(x_j | \text{PA}_j^h) + \sum_{i \in \text{CH}_j^h} \frac{\partial}{\partial x_j} \log p^h(x_i | \text{PA}_i^h) \right] \\
&= \sum_{h=1}^H \frac{w_h p^h(x)}{\sum_{k=1}^H w_k p^k(x)} \left[\frac{\partial}{\partial x_j} \log p_{N_j}^h(x_j - f_j^h(\text{PA}_j^h)) + \sum_{i \in \text{CH}_j^h} \frac{\partial}{\partial x_j} \log p_{N_i}^h(x_i - f_i^h(\text{PA}_i^h)) \right]
\end{aligned} \tag{9}$$

Condition (i). First we will prove condition (i). That is, given a leaf node X_j in all DAGs G^h , X_j is not a shifted node (i.e. an invariant node) if and only if $\text{Var}(\frac{\partial s_j(x)}{\partial x_j}) = 0$.

If x_j is a leaf node in all the DAGs G^h , then $\text{CH}_j^h = \emptyset, \forall h \in [H]$, and we can write eq.(9) as:

$$s_j(x) = \sum_{h=1}^H \frac{w_h p^h(x)}{\sum_{k=1}^H w_k p^k(x)} \frac{\partial}{\partial x_j} \log p_{N_j}^h(x_j - f_j^h(\text{PA}_j^h))$$

We use $\text{Den}(\frac{\partial s_j(x)}{\partial x_j})$ and $\text{Num}(\frac{\partial s_j(x)}{\partial x_j})$ to denote the denominator and numerator of $\frac{\partial s_j(x)}{\partial x_j}$, respectively. Then we have:

$$\text{Den}\left(\frac{\partial s_j(x)}{\partial x_j}\right) = \left(\sum_{k=1}^H w_k p^k(x) \right)^2$$

$$\begin{aligned} \text{Num}\left(\frac{\partial s_j(x)}{\partial x_j}\right) &= \left[\sum_{h=1}^H w_h p^h(x) \frac{\partial^2}{\partial x_j^2} \log p_{N_j}^h(x_j - f_j^h(\text{PA}_j^h)) + w_h p^h(x) \left(\frac{\partial}{\partial x_j} \log p_{N_j}^h(x_j - f_j^h(\text{PA}_j^h)) \right)^2 \right] \\ &\quad \times \left[\sum_{k=1}^H w_k p^k(x) \right] - \left[\sum_{h=1}^H w_h p^h(x) \frac{\partial}{\partial x_j} \log p_{N_j}^h(x_j - f_j^h(\text{PA}_j^h)) \right]^2 \end{aligned}$$

Now, dividing $\text{Num}\left(\frac{\partial s_j(x)}{\partial x_j}\right)$ over $\text{Den}\left(\frac{\partial s_j(x)}{\partial x_j}\right)$, we obtain:

$$\begin{aligned} \frac{\partial s_j(x)}{\partial x_j} &= \frac{\text{Num}\left(\frac{\partial s_j(x)}{\partial x_j}\right)}{\text{Den}\left(\frac{\partial s_j(x)}{\partial x_j}\right)} = \sum_{h=1}^H \frac{w_h p^h(x)}{\sum_{k=1}^H w_k p^k(x)} \frac{\partial^2}{\partial x_j^2} \log p_{N_j}^h(x_j - f_j^h(\text{PA}_j^h)) \\ &\quad + \sum_{h=1}^H \frac{w_h p^h(x)}{\sum_{k=1}^H w_k p^k(x)} \left(\frac{\partial}{\partial x_j} \log p_{N_j}^h(x_j - f_j^h(\text{PA}_j^h)) \right)^2 \\ &\quad - \left[\sum_{h=1}^H \frac{w_h p^h(x)}{\sum_{k=1}^H w_k p^k(x)} \frac{\partial}{\partial x_j} \log p_{N_j}^h(x_j - f_j^h(\text{PA}_j^h)) \right]^2 \end{aligned} \quad (10)$$

Note that since $x_j \notin \text{PA}_j^h$, the function $f_j^h(\text{PA}_j^h)$ is independent of x_j .

Let $a_h = w_h p^h(x)$, and let $b_h = \frac{\partial}{\partial x_j} \log p_{N_j}^h(x_j - f_j^h(\text{PA}_j^h))$. Then, the last two summands of the RHS of eq.(10) can be written as:

$$\frac{1}{\left(\sum_{h=1}^H a_h\right)^2} \left[\left(\sum_{h=1}^H a_h b_h^2\right) \left(\sum_{h=1}^H a_h\right) - \left(\sum_{h=1}^H a_h b_h\right)^2 \right] \geq 0, \quad (11)$$

where the last inequality holds from Lemma 1. Then, by Lemma 3, we have that $b_h = b_{h'} \iff \mathbb{P}^h(X_j | \text{PA}_j^h) = \mathbb{P}^{h'}(X_j | \text{PA}_j^{h'})$ for all $h, h' \in [H]$. Then if $b_h = b_{h'}$ holds, by Lemma 2, we have $c_j^h = c_j^{h'} := c_j$ and then the first term for eq.(10) boils down to a constant c_j . Finally, from Lemma 1, we have that equality in eq.(11) holds if and only if $b_h = b_{h'}$ for all $h, h' \in [H]$. Thus, we conclude that:

$$\text{If } X_j \text{ is a leaf node for all } G^h, \text{ then } X_j \text{ is not a shifted node} \iff \frac{\partial s_j(x)}{\partial x_j} = c_j,$$

where $\frac{\partial s_j(x)}{\partial x_j} = c_j$ is equivalent to $\text{Var}_q\left(\frac{\partial s_j(x)}{\partial x_j}\right) = 0$.

Condition (ii). We now prove that if $\text{Var}_q\left(\frac{\partial s_j(x)}{\partial x_j}\right) > 0$, then only one of the following two cases holds: Case 1) X_j is a leaf node for all G^h and a shifted node. Case 2) X_j is not a leaf node in at least one DAG G^h .

Case 1 follows immediately from the proof of condition (i) above.

For Case 2, we study whether there exists a non-leaf node X_j with $\text{Var}_q\left(\frac{\partial s_j(x)}{\partial x_j}\right) = 0$. Taking the partial derivative of $s_j(x)$ in eq.(9) w.r.t. x_j , we have:

$$\begin{aligned} \frac{\partial s_j(x)}{\partial x_j} &= \sum_{h=1}^H \frac{w_h p^h(x)}{\sum_{k=1}^H w_k p^k(x)} \left(\frac{\partial^2}{\partial x_j^2} \log p_{N_j}^h(x_j - f_j^h(\text{PA}_j^h)) + \sum_{i \in \text{CH}_j^h} \frac{\partial^2}{\partial x_j^2} \log p_{N_i}^h(x_i - f_i^h(\text{PA}_i^h)) \right) \\ &\quad + \sum_{h=1}^H \frac{w_h p^h(x)}{\sum_{k=1}^H w_k p^k(x)} \left(\frac{\partial}{\partial x_j} \log p_{N_j}^h(x_j - f_j^h(\text{PA}_j^h)) + \sum_{i \in \text{CH}_j^h} \frac{\partial}{\partial x_j} \log p_{N_i}^h(x_i - f_i^h(\text{PA}_i^h)) \right)^2 \end{aligned}$$

$$- \left[\sum_{h=1}^H \frac{w_h p^h(x)}{\sum_{k=1}^H w_k p^k(x)} \left(\frac{\partial}{\partial x_j} \log p_{N_j}^h(x_j - f_j^h(\text{PA}_j^h)) + \sum_{i \in \text{CH}_j^h} \frac{\partial}{\partial x_j} \log p_{N_i}^h(x_i - f_i^h(\text{PA}_i^h)) \right) \right]^2$$

By Assumptions **B**, we have $\frac{\partial^2}{\partial x_j^2} \log p_{N_j}^h(x_j - f_j^h(\text{PA}_j^h)) = c_j^h$. For simplicity, let $a_h = \frac{\partial}{\partial x_j} \log p_{N_j}^h(x_j - f_j^h(\text{PA}_j^h)) + \sum_{i \in \text{CH}_j^h} \frac{\partial}{\partial x_j} \log p_{N_i}^h(x_i - f_i^h(\text{PA}_i^h))$. Then, we have:

$$\begin{aligned} \frac{\partial s_j(x)}{\partial x_j} &= \underbrace{\sum_{h=1}^H \frac{w_h p^h(x)}{\sum_{k=1}^H w_k p^k(x)} c_j^h + \sum_{h=1}^H \frac{w_h p^h(x)}{\sum_{k=1}^H w_k p^k(x)} \sum_{i \in \text{CH}_j^h} \frac{\partial^2}{\partial x_j^2} \log p_{N_i}^h(x_i - f_i^h(\text{PA}_i^h))}_{\text{term 1}} \\ &\quad + \underbrace{\sum_{h=1}^H \frac{w_h p^h(x)}{\sum_{k=1}^H w_k p^k(x)} a_h^2 - \left(\sum_{h=1}^H \frac{w_h p^h(x)}{\sum_{k=1}^H w_k p^k(x)} a_h \right)^2}_{\text{term 2}}. \end{aligned} \quad (12)$$

We prove that $\frac{\partial^2}{\partial x_j^2} \log p_{N_i}^h(x_i - f_i^h(\text{PA}_i^h))$, is not constant under any circumstance, by contradiction. Let G^h be an environment's DAG where X_j is not a leaf, and let $X_u \in \text{CH}_j^h$ such that $X_u \notin \cup_{i \in \text{CH}_j^h} \text{PA}_i^h$. Note that X_u always exist since X_j is not a leaf, and it suffices to pick a child X_u appearing at the latest position in the topological order of G^h . Now suppose that $\frac{\partial^2}{\partial x_j^2} \log p_{N_u}^h(x_u - f_u^h(\text{PA}_u^h)) = a$, where a is a constant. Then we have:

$$\begin{aligned} \frac{\partial}{\partial x_j} \log p_{N_u}^h(x_u - f_u^h(\text{PA}_u^h)) &= ax_j + g(x_{-j}), \\ \frac{\partial}{\partial x_j} f_u^h(\text{PA}_u^h) \cdot \frac{\partial}{\partial n_u} \log p_{N_u}^h(n_u) &= ax_j + g(x_{-j}). \end{aligned}$$

By deriving both sides w.r.t. x_u , we obtain:

$$\begin{aligned} \frac{\partial}{\partial x_j} f_u^h(\text{PA}_u^h) \cdot \frac{\partial^2}{\partial n_u^2} \log p_{N_u}^h(n_u) &= \frac{\partial g(x_{-j})}{\partial x_u} \\ \frac{\partial}{\partial x_j} f_u^h(\text{PA}_u^h) \cdot c_j^h &= \frac{\partial g(x_{-j})}{\partial x_u}. \end{aligned}$$

Since the RHS does not depend on x_j , then $\frac{\partial f_u^h}{\partial x_j}$ cannot depend on x_j neither, implying that f_u^h is linear in x_j , thus contradicting the non-linearity assumption (Assumption **A**). Consequently, it becomes evident that term 1 cannot be a constant, regardless of whether the node X_j has undergone a shift or not.

Now let us take a look to term 2 in eq.(12). We have:

$$\sum_{h=1}^H \frac{w_h p^h(x)}{\sum_{k=1}^H w_k p^k(x)} a_h^2 - \left(\sum_{h=1}^H \frac{w_h p^h(x)}{\sum_{k=1}^H w_k p^k(x)} a_h \right)^2 \geq 0,$$

where the inequality follows by Jensen's inequality. Thus we conclude that if X_j is a non-leaf node, we have $\text{Var}_q\left(\frac{\partial s_j(x)}{\partial x_j}\right) > 0$. \square

B.2 Proof of Theorem 2

To proof the theorem we will need the following assumptions:

Assumption C. Let MB_j^h denote the Markov Blanket of node X_j under environment h , then assume

- There are non-negative real number β and C such that for any subset $X_S \subseteq \text{Pre}(X_j^h)$ of size $\leq 1/\delta + 2$, any $x, x' \in \mathbb{R}^{|X_S|}$ and any $t \in \mathbb{R}$,

$$|\mathbb{P}(X_j^h \geq t \mid X_S = x) - \mathbb{P}(X_j^h \geq t \mid X_S = x')| \leq C(1 + \|x\|^\beta + \|x'\|^\beta)\|x - x'\|$$

where $|X_S|$ is the size of the set X_S .

- There are positive numbers C_1 and C_2 such that for any X_S of size $\leq 1/\delta + 2$ and any $t > 0$, $\mathbb{P}(\|X_S\| \geq t) \geq C_1 e^{-C_2 t}$
- For any subset $X_S \subseteq \text{Pre}(X_j^h)$ such that $X_S \subsetneq \text{MB}_j^h$, there exists X_i with $X_i \in \text{MB}_j^h \setminus X_S$, such that for any X_j with $X_j \notin \text{MB}_j^h$,

$$Q(X_S \cup \{X_i\}) - Q(X_S \cup \{X_j\}) \geq \delta/4 \quad Q(X_S) = \int \text{Var}(\mathbb{P}(X_j^h \geq t \mid X_S)) d\mu(t)$$

where δ is the largest number such that for any subset X_S from $\text{Pre}(X_j^h)$, there is some $X_i \notin X_S$ such that $Q(X_S \cup \{X_i\}) \geq Q(X_S) + \delta$.

Proof. Under Assumption **C**, from Theorem 3.1 in [4], we have

$$\mathbb{P}(\widehat{\text{MB}}_j^h = \text{MB}_j^h) \geq 1 - C_3 e^{-C_4 m}$$

where C_3 and C_4 are constants that depend only on the data generation process, and m is the number of samples. Since the estimated topological order $\hat{\pi}$ is assumed to be valid for all environments, we can conclude that node X_j is a leaf node in the input data $\{\text{Pre}(X_j^h), X_j^h\}$ for all h . As a result, we have $\text{MB}_j^h = \text{PA}_j^h$ based on the Markov blanket definition. Therefore, the output of Algorithm 4 is equal to the true parent set PA_j^h with high probability. \square

B.3 Proof of Theorem 3 in Appendix D

To prove Theorem 3 we will make use of the following lemmas.

Lemma 4. Suppose \mathbf{X} is an $n \times k_x$ dimension matrix, \mathbf{Y} is an $n \times k_y$ dimension matrix. Let the columns of the concatenated matrix $\mathbf{Z} = (\mathbf{X}, \mathbf{Y})$ be linearly independent. Consider $\tilde{\beta}_x$, a k_x -dimensional vector, and $\tilde{\beta}_y$ and β_y , both k_y -dimensional vectors. If $\mathbf{X}\tilde{\beta}_x + \mathbf{Y}\tilde{\beta}_y = \mathbf{Y}\beta_y$, then it follows that $\tilde{\beta}_y = \beta_y$ and $\tilde{\beta}_x = \mathbf{0}$.

Proof.

$$\mathbf{X}\tilde{\beta}_x + \mathbf{Y}\tilde{\beta}_y - \mathbf{Y}\beta_y = (\mathbf{X}, \mathbf{Y}) \begin{pmatrix} \tilde{\beta}_x \\ \tilde{\beta}_y \end{pmatrix} - (\mathbf{X}, \mathbf{Y}) \begin{pmatrix} \mathbf{0}_{k_x} \\ \beta_y \end{pmatrix} = \mathbf{Z} \begin{pmatrix} \tilde{\beta}_x \\ \tilde{\beta}_y - \beta_y \end{pmatrix} = \mathbf{0}$$

Since \mathbf{Z} has full column rank, then the null space of \mathbf{Z} is $\mathbf{0}$, which implies $\tilde{\beta}_x = \mathbf{0}$, $\tilde{\beta}_y = \beta_y$. \square

Lemma 5. For any $h \in [H]$, if

$$\sum_{k \in \text{Pre}(X_j)} \Psi_{jk} \tilde{\beta}_{jk}^h = \sum_{k \in \text{PA}_j^h} \Psi_{jk} \beta_{jk}^h,$$

then $\tilde{\beta}_{jk}^h = \beta_{jk}^h$ if $k \in \text{PA}_j^h$, and $\tilde{\beta}_{jk}^h = 0$ if $k \notin \text{PA}_j^h$.

Proof. Rearrange the set $\text{Pre}(X_j)$ so that $\text{Pre}(X_j) = \{X_{k_1}, X_{k_2}, \dots, X_{k_m}, X_{k_{m+1}}, \dots, X_{k_p}\}$, where $\{X_{k_1}, \dots, X_{k_m}\} = \text{Pre}(X_j) \setminus \text{PA}_j$, and $\{X_{k_{m+1}}, \dots, X_{k_p}\} = \text{PA}_j$. Then let $\mathbf{X} = (\Psi_{k_1}, \dots, \Psi_{k_m})$, $\mathbf{Y} = (\Psi_{k_{m+1}}, \dots, \Psi_{k_p})$, and $\mathbf{Z} = (\mathbf{X}, \mathbf{Y})$. By the linear independence property of the basis functions of $\text{Pre}(X_j)$, we have that the columns of \mathbf{Z} are linearly independent. Also, let

$$\tilde{\beta}_x = \begin{pmatrix} \tilde{\beta}_{jk_1}^h \\ \vdots \\ \tilde{\beta}_{jk_m}^h \end{pmatrix}, \quad \tilde{\beta}_y = \begin{pmatrix} \tilde{\beta}_{jk_{m+1}}^h \\ \vdots \\ \tilde{\beta}_{jk_p}^h \end{pmatrix}, \quad \beta_y = \begin{pmatrix} \beta_{jk_{m+1}}^h \\ \vdots \\ \beta_{jk_p}^h \end{pmatrix}$$

Then we must have:

$$\sum_{k \in \text{Pre}(X_j)} \Psi_{jk} \tilde{\beta}_{jk}^h = \sum_{k \in \text{PA}_j^h} \Psi_{jk} \beta_{jk}^h \Rightarrow \mathbf{X} \tilde{\beta}_x + \mathbf{Y} \tilde{\beta}_y = \mathbf{Y} \beta_y.$$

Then by Lemma 4, we have $\tilde{\beta}_{jk}^h = \beta_{jk}^h$ if $k \in \text{PA}_j^h$, $\tilde{\beta}_{jk}^h = 0$ if $k \notin \text{PA}_j^h$. \square

Proof of Theorem 3. We know that $\text{Pre}(X_j)$ contains the ancestors of X_j . Then, in environment h , we have:

$$\begin{aligned} \mathbb{E}_{p^h}[X_j | \text{Pre}(X_j)] &= \mathbb{E}_{p^h}[f_j^h(\text{PA}_j^h) | \text{Pre}(X_j)] + \mathbb{E}_{p^h}[N_j | \text{Pre}(X_j)] \\ &= f_j^h(\text{PA}_j^h), \end{aligned}$$

where the last equality follows since the first conditional expectation is equal to $f_j^h(\text{PA}_j^h)$, due to $\text{PA}_j \subseteq \text{Pre}(X_j)$. Moreover, in the second conditional expectation term, we have that N_j is marginally independent of $\text{Pre}(X_j)$ by the d-separation criterion. Thus the conditional expectation of N_j equals to the marginal expectation of N_j , which is 0. Finally,

$$\sum_{k \in \text{Pre}(X_j)} \Psi_{jk} \tilde{\beta}_{jk}^h = \mathbb{E}_{p^h}[X_j | \text{Pre}(X_j)] = f_j^h(\text{PA}_j^h) = \sum_{k \in \text{PA}_j^h} \Psi_{jk} \beta_{jk}^h$$

By Lemma 5, we have $\tilde{\beta}_{jk}^h = \beta_{jk}^h$ if $k \in \text{PA}_j^h$, $\tilde{\beta}_{jk}^h = 0$ if $k \notin \text{PA}_j^h$. \square

C Additional Experiments

This section provides a thorough evaluation of the pipeline of our method. We begin by assessing the performance of our method in detecting the shifted nodes. Subsequently, we extend the evaluation to include the recovery of the structurally shifted edges.

C.1 Experiments on detecting shifted nodes

Graph models. We ran experiments by generating adjacency matrices using the Erdős–Rényi (ER) and Scale free (SF) graph models. For a given number of variables d , ER k and SF k indicate an average number of edges equal to kd .

Data generation process. We first sampled a Directed Acyclic Graph (DAG) according to either the Erdős–Rényi (ER) model or the Scale-Free (SF) model for environment \mathcal{E}_1 .

For environment \mathcal{E}_2 , we used the same DAG structure as in environment \mathcal{E}_1 , ensuring a direct comparison between the two environments. To introduce artificial shifted nodes, we randomly selected $0.2 \cdot d$ nodes from the non-root nodes, where d represents the total number of nodes in the DAG. These selected nodes were considered as the "shifted nodes," denoted as S , with $|S| = 0.2d$.

The functional relationship between a node X_j and its parents in environment \mathcal{E}_1 was defined as follows:

$$X_j = \sum_{i \in \text{PA}_j} \sin(X_i^2) + N_j,$$

while for environment \mathcal{E}_2 , we defined the functional relationships between each node and its parents by:

$$X_j = \begin{cases} \sum_{i \in \text{PA}_j} \sin(X_i^2) + N_j, & \text{if } X_j \notin S, \\ \sum_{i \in \text{PA}_j} 4 \cos(2X_i^2 - 3X_i) + N_j, & \text{if } X_j \in S. \end{cases}$$

Experiment detail. In each simulation, we generated 500 data points, with the variances of the noise set to 1. We conducted 30 simulations for each combination of graph type, noise type, and number of nodes. The running time was recorded by executing the experiments on an Intel Xeon Gold 6248R Processor with 8 cores. For our method, we used the hyperparameters $\text{eta_G} = 0.005$, $\text{eta_H} = 0.005$, and threshold $t = 2$ (see Algorithm 3).

Evaluation. We conducted a comparative analysis to evaluate the performance of our method in detecting shifted nodes compared to DCI. The evaluation was based on F1 score, precision, and recall as the evaluation metrics. Furthermore, we examined the robustness of our method by conducting tests using Gumbel and Laplace as noise distributions.

Figures 6, 7, and 8 illustrate our method’s performance across varying numbers of nodes and sparsity levels of the graphs. Our method consistently outperformed DCI in terms of F1 score, precision, and recall.

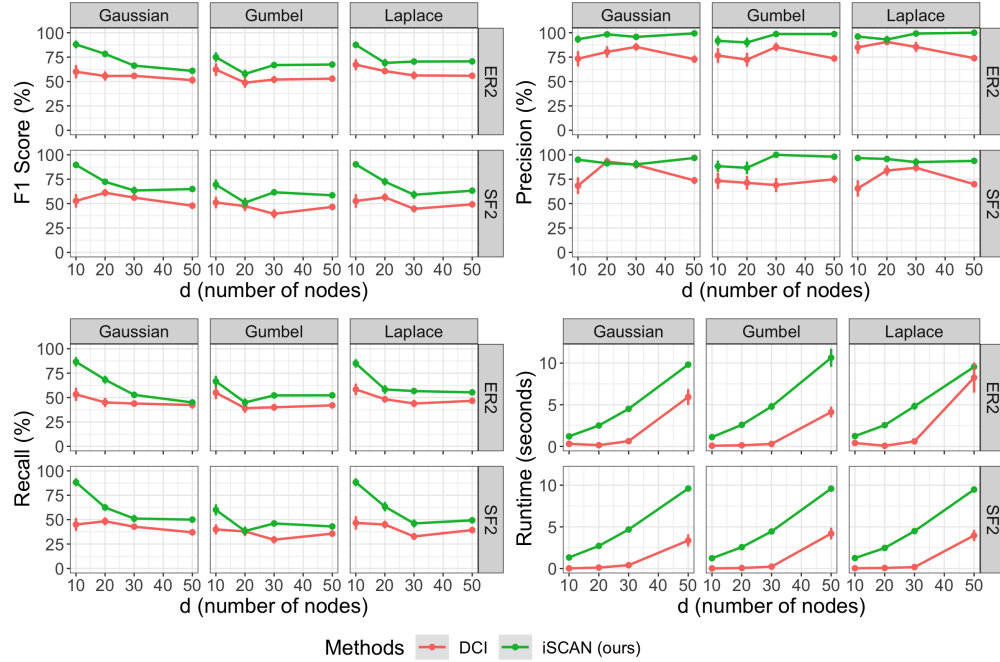


Figure 6: Shifted nodes detection in ER2 and SF2 graphs. For each point, we conducted 30 simulations as described in Section C.1. The points indicate the average values obtained from these simulations, while the error bars depict the standard errors. For each simulation, 500 samples were generated. Our method iSCAN (green) consistently outperformed DCI (red) in terms of F1 score, precision, and recall.

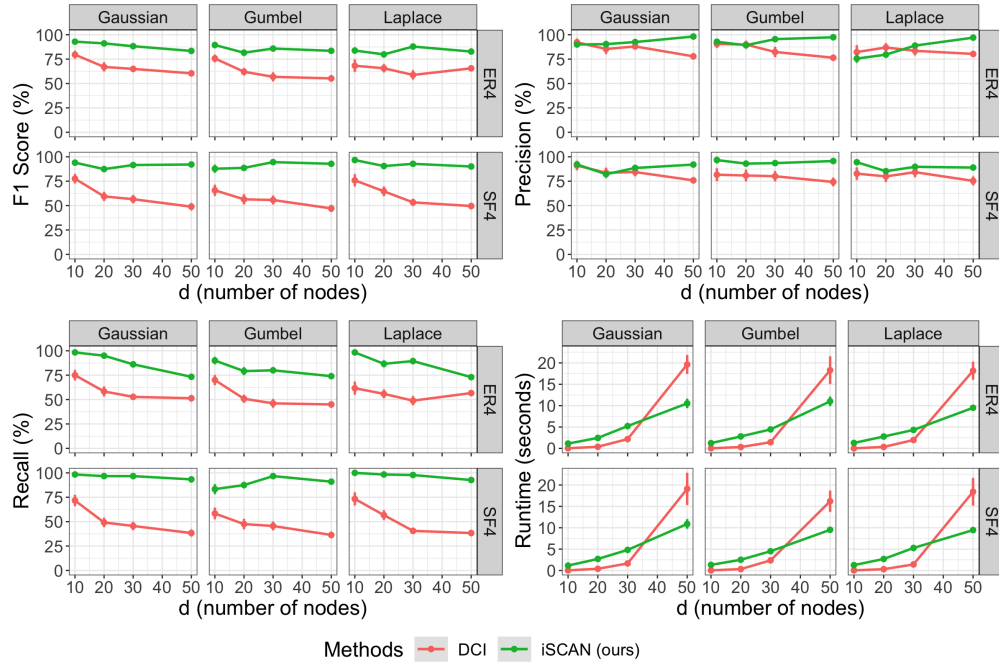


Figure 7: Shifted nodes detection in ER4 and SF4 graphs. For each point, we conducted 30 simulations as described in Section C.1. The points indicate the average values obtained from these simulations, while the error bars depict the standard errors. For each simulation, 500 samples were generated. Our method iSCAN (green) consistently outperformed DCI (red) in terms of F1 score, precision, and recall.

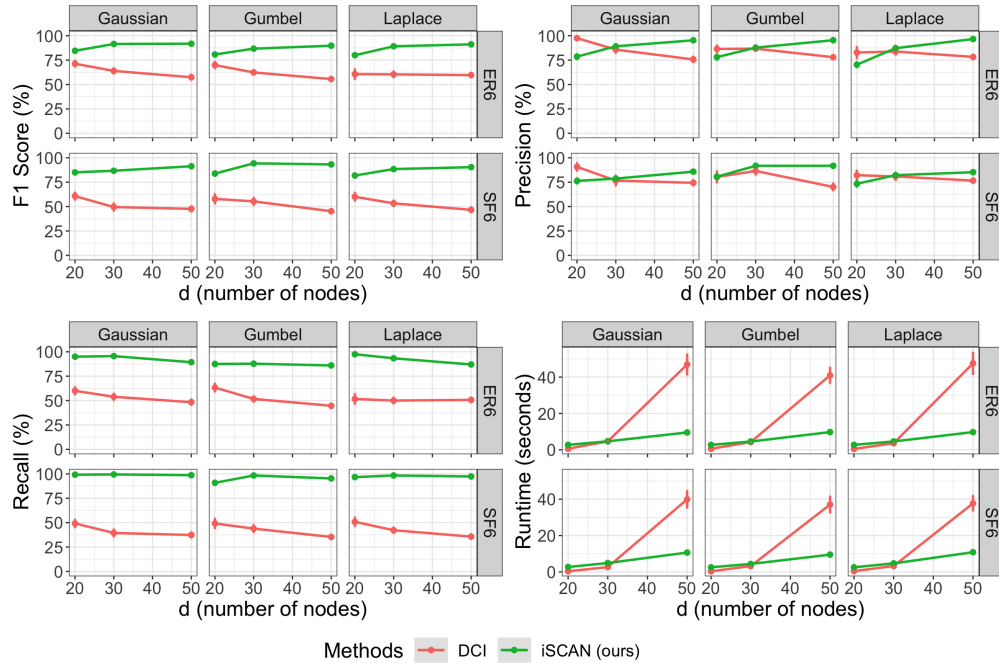


Figure 8: Shifted nodes detection in ER6 and SF6 graphs. For each point, we conducted 30 simulations as described in Section C.1. The points indicate the average values obtained from these simulations, while the error bars depict the standard errors. For each simulation, 500 samples were generated. Our method iSCAN (green) consistently outperformed DCI (red) in terms of F1 score, precision, and recall.

C.1.1 Experiments in detecting shifted nodes from Gaussian process

Data generation process. We first sampled a DAG according to the ER or SF model. In our experiment, we considered two environments, \mathcal{E}_1 and \mathcal{E}_2 , with the same DAG structure. Each node in the graph had a functional relationship with its parents defined as $X_j = f_j^h(\text{PA}_j^h) + N_j$, where N_j is an independent standard Gaussian variable. Recall that the superscript h denotes the function for environment \mathcal{E}_h .

To introduce shifted nodes, we randomly selected $0.2 \cdot d$ nodes from the non-root nodes, denoted as S , to be the shifted nodes. In other words, $|S| = 0.2d$. For the non-shifted nodes X_j (i.e. $j \notin S$), we set $f_j^1 = f_j^2$. However, for each shifted node X_j in S , we changed its functional relationship with its parents to $X_j = 2 \cdot f_j^2(\text{PA}_j^2) + N_j$.

To test our method in a more general setting involving nonlinear functions, we followed the approach in [65, 39]. Specifically, for *non-shifted nodes*, we generated the link functions f_j^1 by sampling Gaussian processes with a half unit bandwidth RBF kernel, and we set $f_j^2 = f_j^1$. For *shifted nodes*, $X_j \in S$, we generated the link functions f_j^1 and f_j^2 by sampling Gaussian processes with a half unit bandwidth RBF kernel independently. This allowed us to simulate different functional relationships for the shifted nodes across the two environments.

Experiment detail. In each simulation, we generated 1000 data points, with the variances of the noise set to 1. We conducted 30 simulations for each combination of graph type, noise type, and number of nodes. The running time was recorded by executing the experiments on an Intel Xeon Gold 6248R Processor with 8 cores. For our method, we used the hyperparameters `eta_G = 0.005`, `eta_H = 0.005`, and `elbow = True` (see Remark 6).

Evaluation. We conducted a comparative performance analysis between our proposed Algorithm 1 (iSCAN, green) and the DCI (red) method. The results for ER2 and SF2 graphs under Gaussian, Gumbel, and Laplace noise distributions are shown in Figure 9. In certain cases, our method may underperform DCI in terms of precision, resulting in a lower F1 score. However, it is important to note that our method consistently outperforms DCI in terms of recall score.

Furthermore, Figure 10 and Figure 11 present the results for ER4/SF4, and ER6/SF6 graphs. In terms of precision, our method exhibits competitive performance and, in many cases, outperforms DCI. Notably, iSCAN consistently surpasses DCI in terms of recall score and F1 score.

These findings emphasize the strengths of our proposed method in accurately detecting shifted nodes and edges, particularly in terms of recall and overall performance. In denser graphs, our method demonstrates a superior ability to recover shifted nodes compared to DCI. This suggests that our method is well-suited for scenarios where the graph structure is more complex and contains a larger number of nodes and edges. The improved performance of our method in such settings further highlights its potential in practical applications and its ability to handle more challenging tasks.

Top-k precision. We have observed that in some cases, the precision of our method underperformed DCI. We attribute this to the elbow method rather than stats_L . To further investigate this, we conducted an analysis using only stats_L and measured the precision based on different criteria. Specifically, we identified nodes as shifted if their stats_L ranked first, first two, or within the top k , denoted as top-1 precision, top-2 precision, and top- k precision, respectively, where $k = |S|$.

Figure 12 presents the results of precision for top-1, top-2, and top- k criteria under various graph models and noise combinations. In most cases, the precision exceeds 80% and even approaches 100%. These results indicate that when using stats_L alone, our method still provides accurate information about shifted nodes. The findings suggest that the lower precision observed in Figure 9 can be attributed to the elbow strategy rather than the effectiveness of stats_L . Overall, this analysis strengthens the reliability and usefulness of stats_L in accurately identifying shifted nodes in our method.

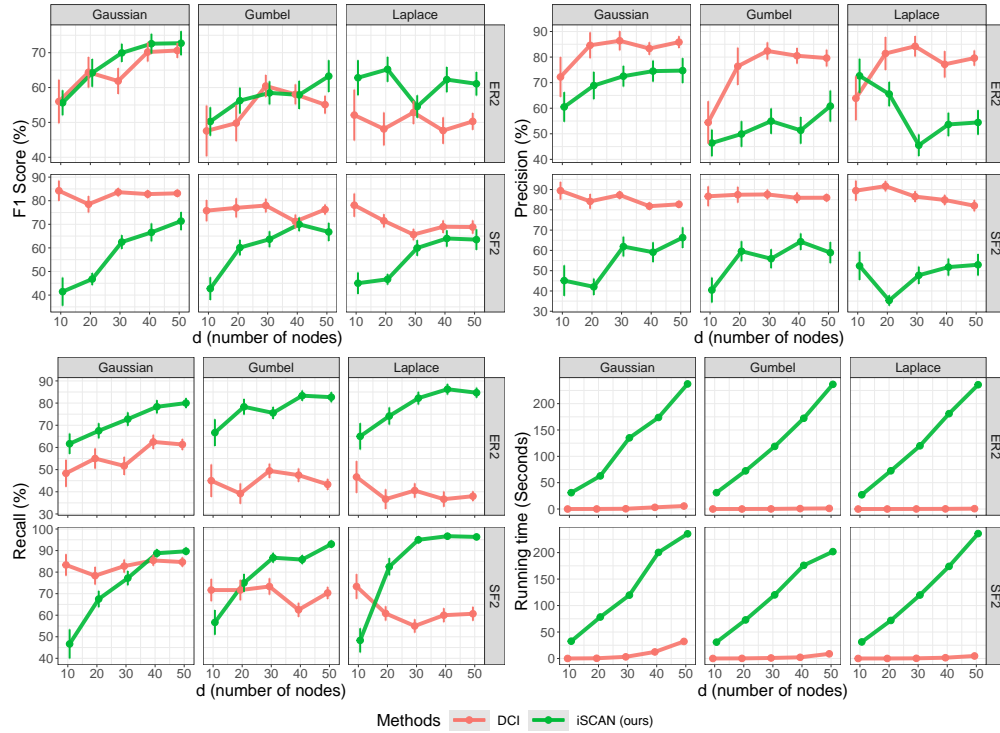


Figure 9: Experiments on detection of shifted nodes in ER2/SF2 graphs using Gaussian processes. Details described in Appendix C.1.1. The error bars represent the standard errors.

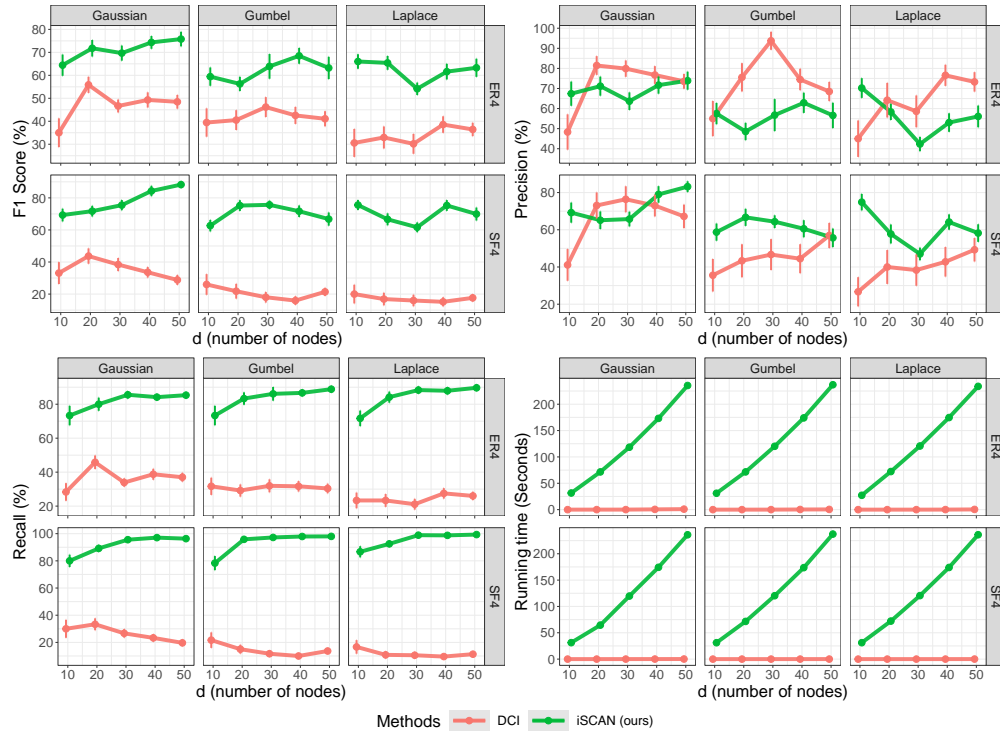


Figure 10: Experiments on detection of shifted nodes in ER4/SF4 graphs using Gaussian processes. Details described in Appendix C.1.1. The error bars represent the standard errors.

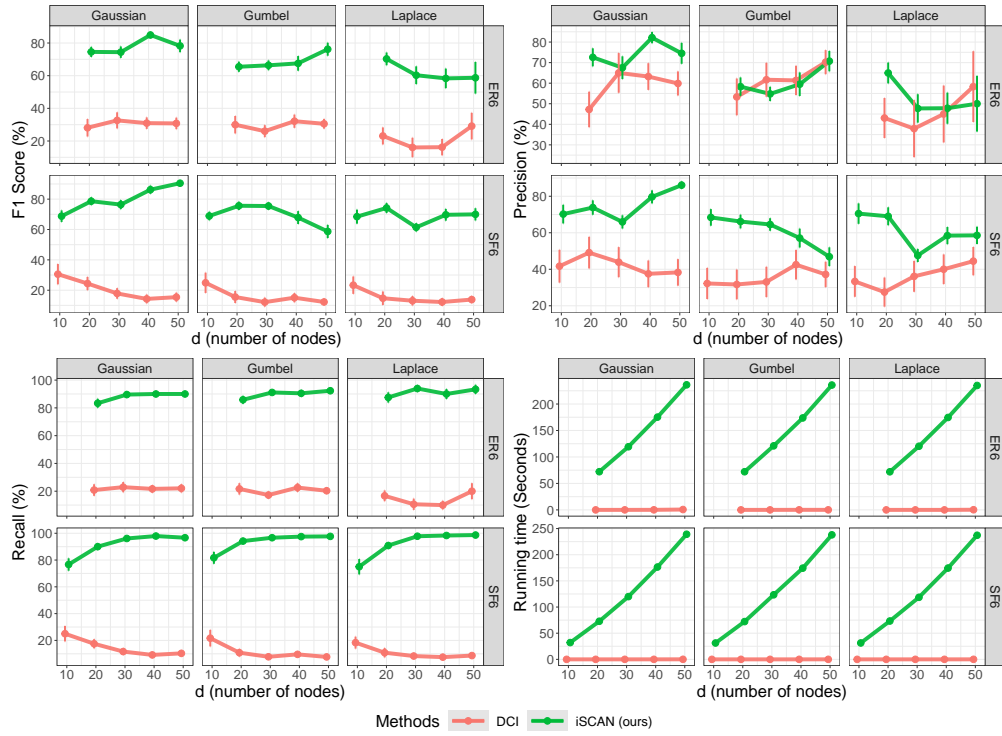


Figure 11: Experiments on detection of shifted nodes in ER6/SF6 graphs using Gaussian processes. Details described in Appendix C.1.1. The error bars represent the standard errors.

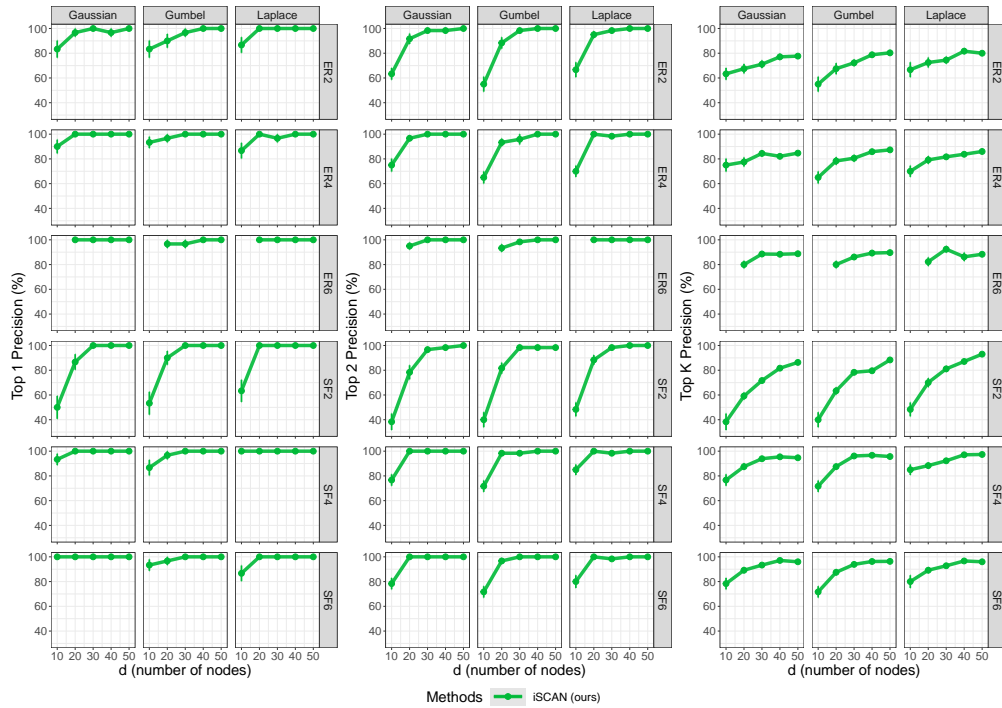


Figure 12: Top 1, 2 and K performance of iSCAN where functionals are sampled from Gaussian processes. Details described in Appendix C.1.1. The error bars represent the standard errors.

C.2 Experiments on estimating structural shifts

Data generation. We first sampled a DAG, G^1 , of d nodes according to either the ER or SF model for env. \mathcal{E}_1 . For env. \mathcal{E}_2 , we initialized its DAG structure from env. \mathcal{E}_1 and produced structural changes by randomly selecting $0.2 \cdot d$ nodes from the non-root nodes. This set of selected nodes S , with cardinality $|S| = 0.2d$, correspond to the set of “shifted nodes”. In env. \mathcal{E}_2 , for each shifted node $X_j \in S$, we uniformly at random deleted at most three of its incoming edges, and use D_j to denote the parents whose edges to X_j were deleted; thus, the DAG G^2 is a subgraph of G^1 . Then, in \mathcal{E}_1 , each X_j was defined as follows:

$$X_j = \sum_{i \in \text{PA}_j^1 \setminus D_j} \sin(X_i^2) + \sum_{i \in D_j} 4 \cos(2X_i^2 - 3X_i) + N_j$$

In \mathcal{E}_2 , each X_j was defined as follows:

$$X_j = \sum_{i \in \text{PA}_j^2} \sin(X_i^2) + N_j$$

Experiment details. For each simulation, we generated 500 data points per environment, i.e., $m_1 = 500, m_2 = 500$ and $m = 1000$. The noise variances were set to 1. We conducted 30 simulations for each combination of graph type (ER or SF), noise type (Gaussian, Gumbel, and Laplace), and number of nodes ($d \in \{10, 20, 30, 50\}$). The running time was recorded by executing the experiments on an Intel Xeon Gold 6248R Processor with 8 cores. For our method, we used $\eta = 0.05$ for eq.(6) and eq.(7), and a threshold $t = 2$ (see Alg. 3).

In the case of the method introduced by Budhathoki et al. [11], we employed Kernel Conditional Independence (KCI) tests [86] for conducting conditional independence tests. As for CITE, KCD, UT-IGSP, and SCORE, we used their respective default parameter settings provided within their packages. Additionally, for SCORE, we employed it to estimate the DAGs independently for different environments and then compared the recovered DAGs to identify the shifted nodes. Given that Budhathoki’s and KCD methods require information about the parents PA_j for each node X_j , we employed the SCORE method to find the parent sets PA_j .

Evaluation. In this experiment, we assessed the performance of our method in two aspects: detecting shifted nodes and recovering the structural changes (**difference DAG**). For the evaluation of shifted node detection, we measured F1 score, recall, and precision. In the evaluation of difference DAG recovery, we compared the estimated difference DAG with the ground truth difference DAG using F1 score. Additionally, we considered the running time of the methods as another evaluation criterion.

Figures 13, 14, and 15 illustrate our method’s performance in detecting shifted nodes across varying numbers of nodes and sparsity levels of the graphs. Our method consistently outperformed baselines in terms of F1 score, precision, and recall.

Figures 16 showcase the performance of our method in recovering difference DAG across different noise distribution, different numbers of nodes and sparsity levels in the graphs. Our method achieves higher F1 score in recovering the difference DAG compared with DCI.

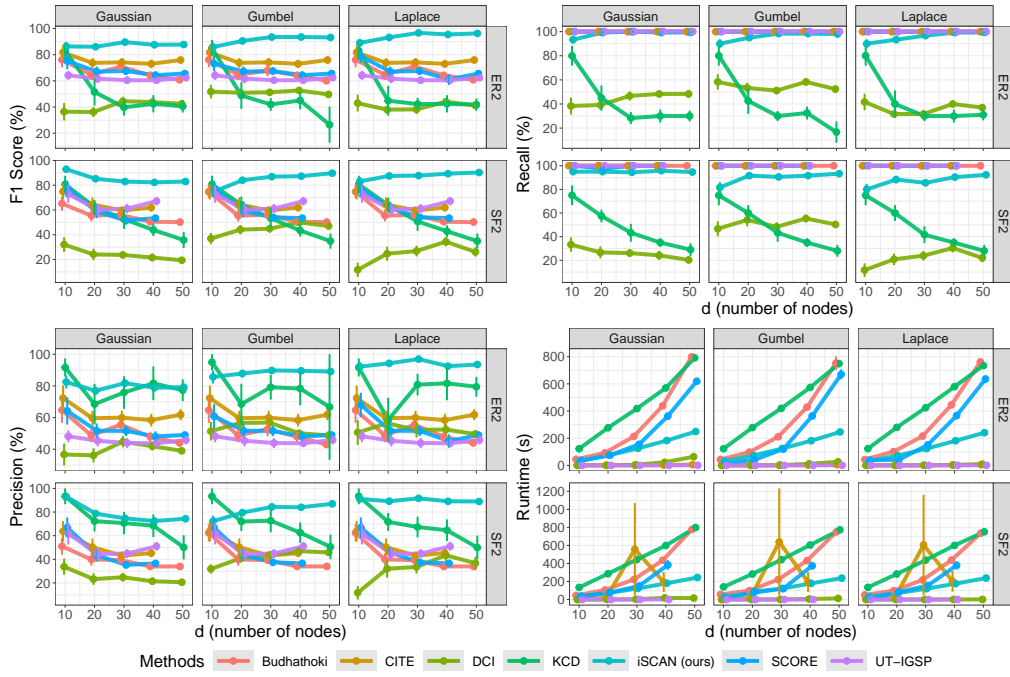


Figure 13: Shifted nodes detection performance in ER2/SF2. See App. C.2 for experimental details. iSCAN (light blue) consistently outperformed baselines in terms of F1 score, precision, and recall.

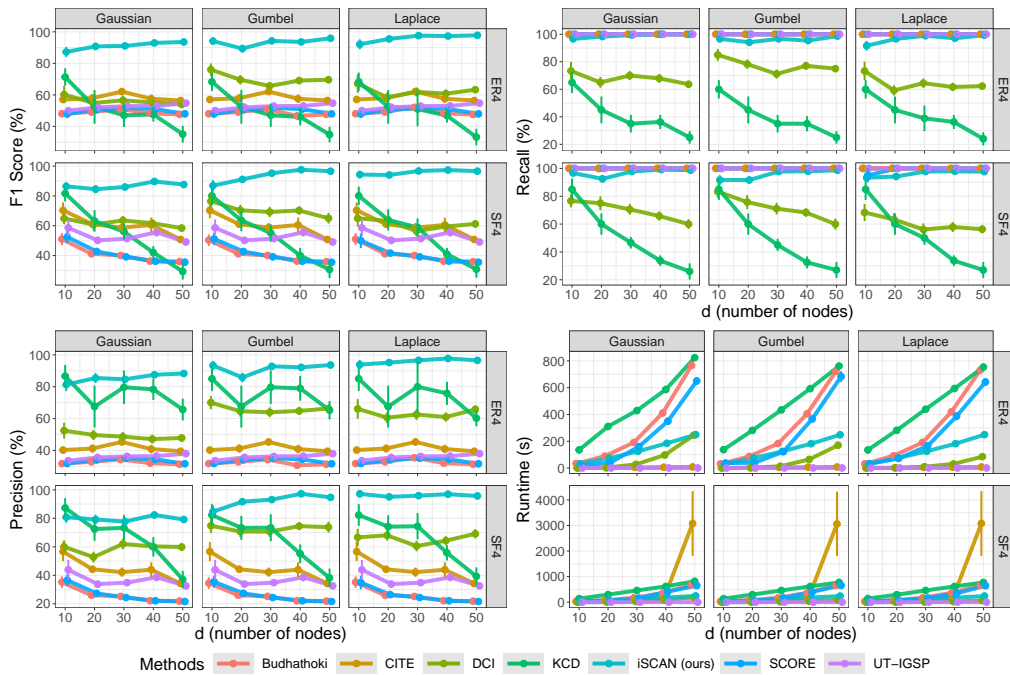


Figure 14: Shifted nodes detection performance in ER4/SF4. See App. C.2 for experimental details. iSCAN (light blue) consistently outperformed baselines in terms of F1 score, precision, and recall.

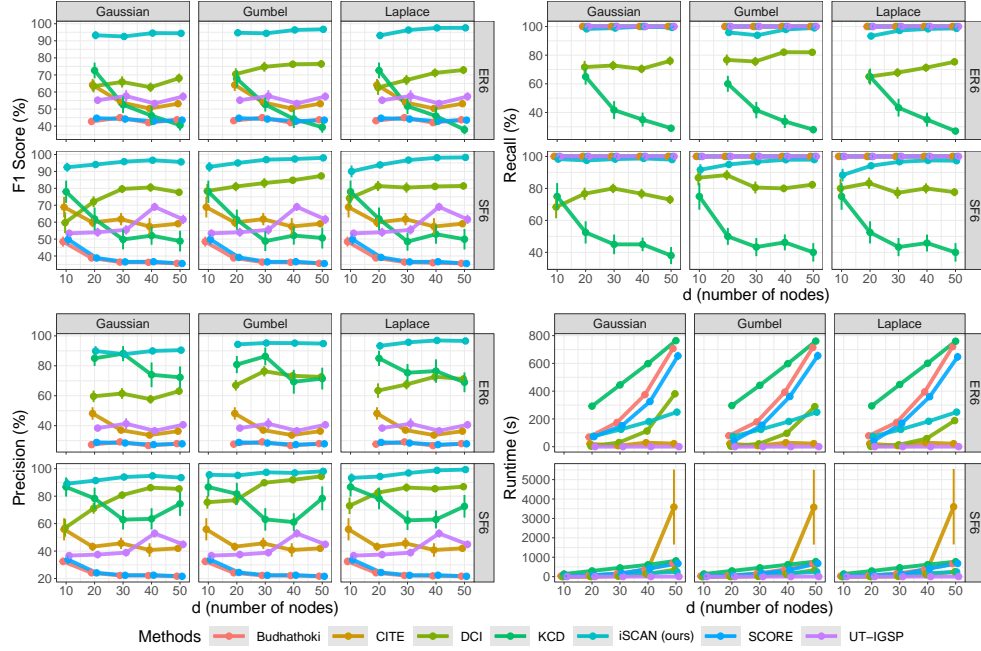


Figure 15: Shifted nodes detection performance in ER6/SF6. See App. C.2 for experimental details. iSCAN consistently outperformed baselines in terms of F1 score, precision, and recall.

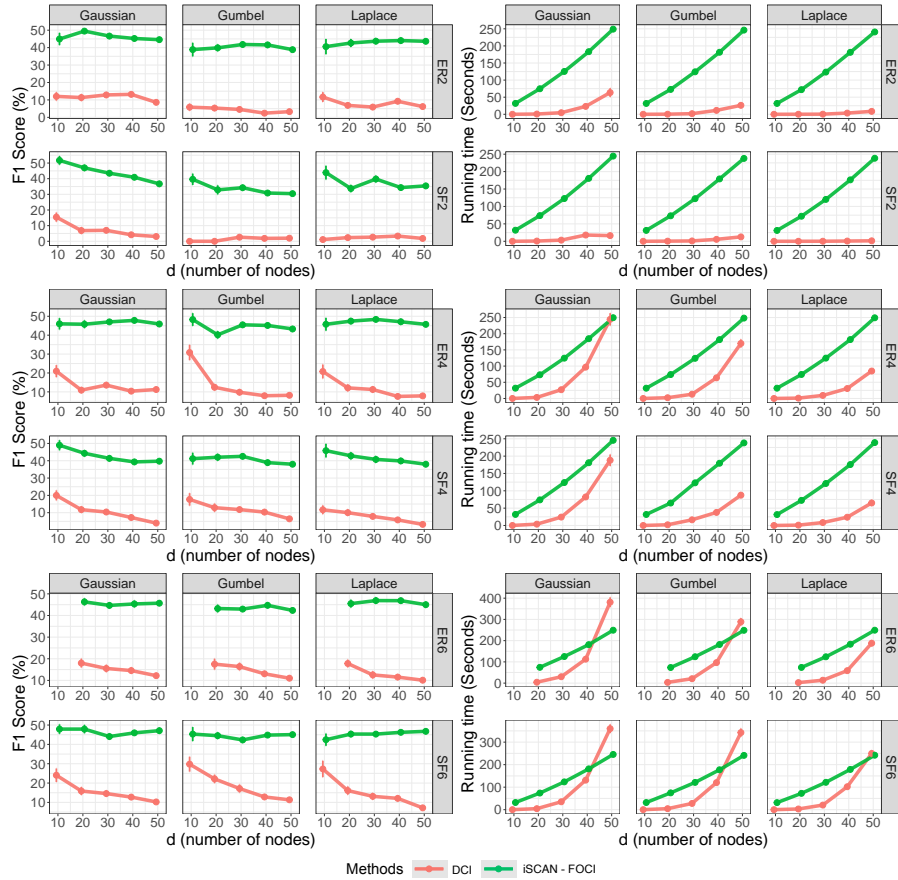


Figure 16: Difference DAG recovery performance in all different graphs. iSCAN-FOCI (green) consistently outperformed DCI (red) in terms of F1 score.

C.3 Performance of Alg. 3 using the elbow method

In this section, we aim to understand the performance of our method when using the elbow approach discussed in Remark 6, random functions for shifted nodes, and different noise variances per variable within an environment.

Data generation process. We first sampled a Directed Acyclic Graph (DAG) according to either the Erdős-Rényi (ER) model or the Scale-Free (SF) model for environment \mathcal{E}_1 .

For environment \mathcal{E}_2 , we used the same DAG structure as in environment \mathcal{E}_1 , ensuring a direct comparison between the two environments. To introduce artificial shifted edges, we randomly selected $0.2 \cdot d$ nodes from the non-root nodes, where d represents the total number of nodes in the DAG. These selected nodes correspond to shifted nodes, denoted as S , with $|S| = 0.2d$. For each shifted node $X_j \in S$, we uniformly and randomly deleted 3 edges originating from its parents for environment \mathcal{E}_2 . The parent nodes whose edges to X_j were deleted are denoted as D_j .

The functional relationship between shifted node X_j and its parents D_j in environment \mathcal{E}_1 was defined as follows:

$$X_j = \sum_{i \in \text{PA}_j, i \notin D_j} \sin(X_i^2) + \sum_{i \in D_j} c_{ij} \cdot f_{ij}(-2X_i^3 + 3X_i^2 + 4X_i) + N_j,$$

where $c_{ij} \sim \text{Uniform}([-5, -2] \cup [2, 5])$, and f_{ij} is a function from $\{\text{sinc}(\cdot), \text{cos}(\cdot)\}$ chosen uniformly at random. For environment \mathcal{E}_2 , where the adjacency matrix has undergone deletions, we defined the functional relationship between each node and its parents as follows:

$$X_j = \sum_{i \in \text{PA}_j} \sin(X_i^2) + N_j$$

Experiment detail. In each simulation, we generated $\{500, 1000\}$ data points, with the variances of the noises set uniformly at random in $[0.25, 0.5]$. We tested three types of noise distributions, namely, the Normal, Laplace, and Gumbel distributions. We conducted a 100 simulations for each combination of graph type, noise type, and number of nodes. The running time was recorded by executing the experiments on an Intel Xeon Gold 6248R Processor with 8 cores. For our method, we used the hyperparameter $\eta = 0.001$. Different from the hard threshold of $t = 2$ used in previous experiments, we now used the elbow approach to determine the set of shifted nodes. To automatically select the elbow we made use of the Python package `Kneed`⁷, with hyperparameters `curve='convex'`, `direction='decreasing'`, `online=online`, `interp_method='interp1d'`.

Evaluation. In this experiment, we assessed the performance of our method in two aspects: detecting shifted nodes and recovering the difference DAG. For the evaluation of shifted node detection, we measured F1 score, recall, and precision. In the evaluation of difference DAG recovery, we compared the estimated difference DAG with the ground truth difference DAG using F1 score.

In Figures 17 and 18 we present the performances when using the elbow approach discussed in Remark 6. In Figure 17, we note that iSCAN performs similarly for number of samples 500 and 1000. We also show the top-1, top-2, and top-k precision of iSCAN when choosing the first, first 2, and first k variables of `stats` (see Algorithm 3) after sorting in decreasing order, respectively. We remark that the superbly performance of iSCAN in top-1 or top-2 precision suggests that in situations that is difficult to choose a threshold for Algorithm 3, the practioner can consider that the first or first two variables of `stats` are more likely to be shifted nodes. Finally, in Figure 18 we show that iSCAN outperforms DCI in recovering the underlying structural difference.

⁷We used the latest version found at: <https://kneed.readthedocs.io/en/stable/>.

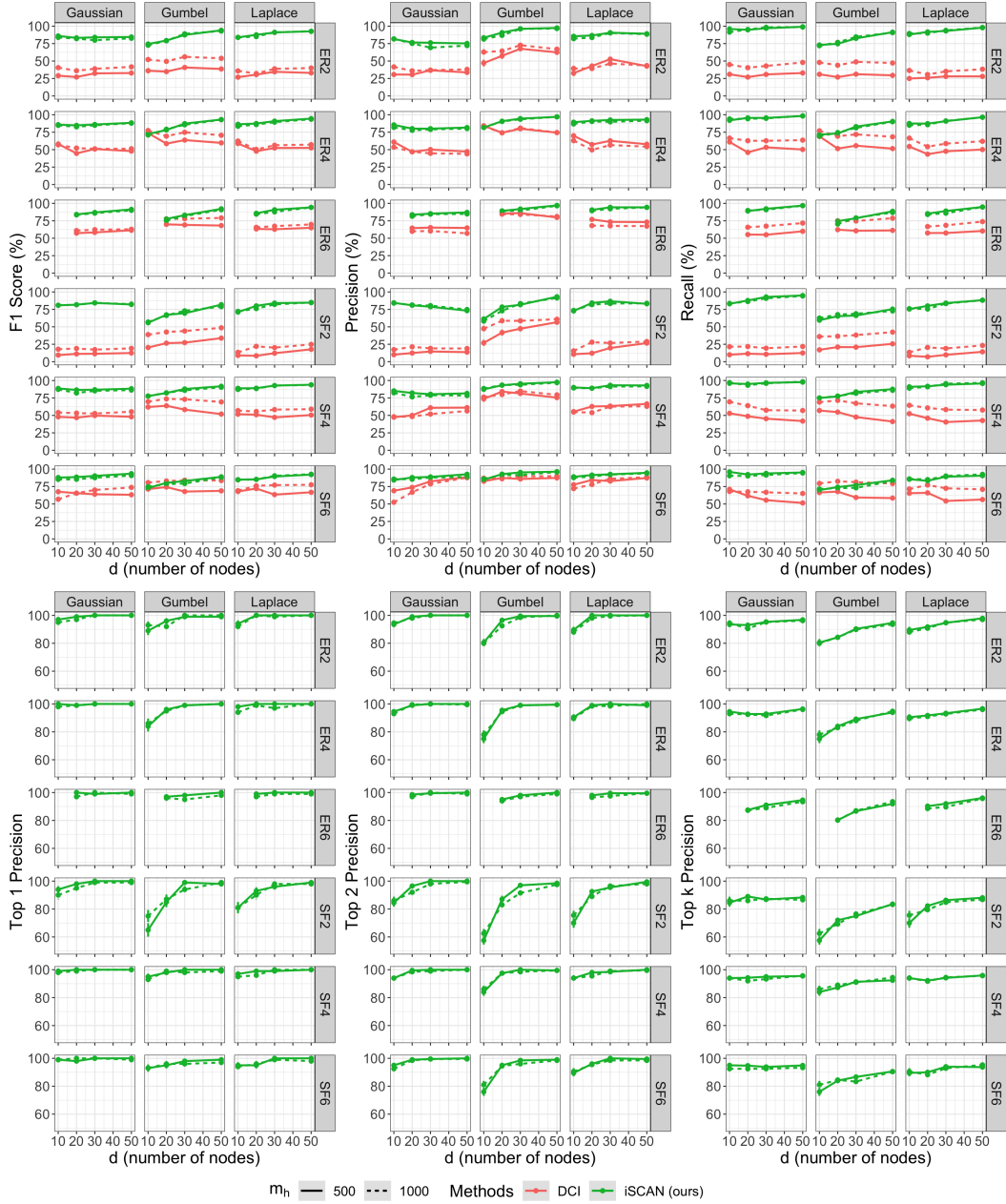


Figure 17: Shifted nodes detection performance in ER k and SF k for $k \in \{2, 4, 6\}$. For each point in each subplot, we conducted 100 simulations as described in Section C.3. The points indicate the average values obtained from these simulations. The error bars depict the standard errors. Our method iSCAN (green) consistently outperformed DCI (red) in terms of F1 score, precision, and recall.

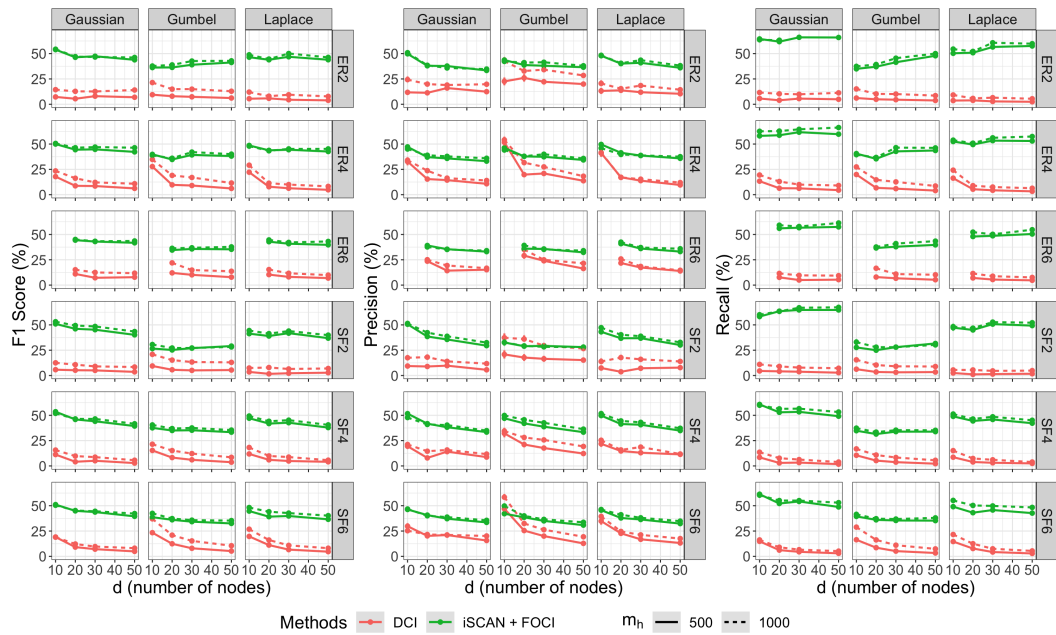


Figure 18: Difference DAG recovery performance in all different graphs. For each point in each subplot, we conducted 100 simulations as described in Section C.3. The points indicate the average values obtained from these simulations. The error bars depict the standard errors. Our method iSCAN with FOCI (green) consistently outperformed DCI (red) in terms of F1 score.

D Additional Discussion on Shifted Edges

In Section 4, we focused on estimating structural changes across the environments (Definition 4). However, in some situations it might be of interest to determine whether the *functional relationship* between two variables has changed across the environments. The latter could have multiple interpretations, in this section, we elaborate on a particular type of functional change via partial derivatives.

Definition 5 (functionally shifted edge). *Given environments $\mathcal{E} = (X, f^h, \mathbb{P}_N^h)$ for $h \in [H]$, an edge $(X_i \rightarrow X_j)$ is called a functionally shifted edge if there exists $h, h' \in [H]$ such that:*

$$\frac{\partial}{\partial x_i} f_j^h(\text{PA}_j^h) \neq \frac{\partial}{\partial x_i} f_j^{h'}(\text{PA}_j^{h'}).$$

Without further assumptions about the functional form of f_j^h , certain ill-posed situations may arise under Definition 5. Let us consider the following example.

Example 1. *Let \mathcal{E}_A and \mathcal{E}_B be two environments, each consisting of three nodes. Let the structural equations for node X_3 be: $X_3^A = \exp(X_1^A + X_2^A) + N_3$, and $X_3^B = \exp(2 \cdot X_1^B + X_2^B) + N_3$. In this scenario, one could consider that the causal relationship $X_2 \rightarrow X_3$ has not changed. However, we note that $\frac{\partial f_3^A}{\partial x_2^A} \neq \frac{\partial f_3^B}{\partial x_2^B}$, thus, testing for changes in the partial derivative would yield a false discovery for the non-shifted edge $X_2 \rightarrow X_3$.*

Ill-posed situations such as the above example can be avoided by additional assumptions on the functional mechanisms. We next discuss a sufficient condition where the partial derivative test for functional changes is well-defined.

Assumption D (Additive Models). *Let S be the set of shifted nodes across all the H environments. Then, for all $j \in S, h \in [H]$:*

$$f_j^h(\text{PA}_j^h) = a_j^h + \sum_{k \in \text{PA}_j^h} f_{jk}^h(X_k),$$

where a_j^h is a constant, f_{jk}^h is a nonlinear function, where $f_{jk}^h(\cdot)$ lies in some space of function class \mathcal{F} .

Remark 7. *Assumption D amounts to modelling each variable as a generalized linear model [27]. It is widely used in nonparametrics and causal discovery [12, 43, 80]. Moreover, it not only provides a practical framework but also makes the definition of shifted edges (as per Definition 5) well-defined and reasonable.*

Remark 8. *Note that Assumption D makes assumptions only on the set of shifted nodes. This is because the set of invariant nodes can be identified regardless of the their type of structural equation, and it is also clear these nodes cannot have any type of shift.*

Now consider a function class \mathcal{F} , which incorporates the use of basis functions to model the additive components f_{jk}^h . Specifically, we express $f_{jk}^h(x_k) = \Psi_{jk}^h(x_k) \beta_{jk}^h$, where feature mapping Ψ_{jk}^h is a $1 \times r$ matrix whose columns represent the basis functions and β_{jk}^h is an r -dimensional vector containing the corresponding coefficients. Moreover we assume that the functions $f_{jk}^1, \dots, f_{jk}^H$ share a same feature mapping $\Psi_{jk}^1(\cdot), \dots, \Psi_{jk}^H(\cdot)$ but can have different coefficients β_{jk}^h across the H environments. The latter has been assumed in prior work, e.g., [44]. The approach of using a basis function approximation is widely adopted in nonparametric analysis, and it has been successfully employed in various domains such as graph-based methods [80], and the popular CAM framework [12]. Then, under Assumption D and Definition 5, we present the following proposition:

Proposition 2. *Under Assumption D, an edge $(X_i \rightarrow X_j)$ is a functionally shifted edge, as in Definition 5, if and only if the basis coefficients are different. That is,*

$$\frac{\partial f_j^h}{\partial x_i} \neq \frac{\partial f_j^{h'}}{\partial x_i} \iff \beta_{ji}^h \neq \beta_{ji}^{h'}.$$

Proof. We have,

$$\frac{\partial f_j^h}{\partial x_i} = \frac{df_{ji}^h(x_i)}{dx_i} = \frac{d(\Psi_{ji}^h(x_i) \beta_{ji}^h)}{dx_i} = \frac{d\Psi_{ji}^h(x_i)}{dx_i} \beta_{ji}^h.$$

Then,

$$\frac{\partial f_j^h}{\partial x_i} - \frac{\partial f_j^{h'}}{\partial x_i} = \frac{d\Psi_{ji}(x_i)}{dx_i}(\beta_{ji}^h - \beta_{ji}^{h'}) \neq \mathbf{0} \iff \beta_{ji}^h - \beta_{ji}^{h'} \neq \mathbf{0}$$

The last \iff relation is due to the linear independence of the basis functions Ψ_{ji} , then the null space of $d\Psi_{ji}/dx_i$ can only be the zero vector $\mathbf{0}$. \square

Note that the output of Algorithm 1 also estimates a topological order $\hat{\pi}$. However, the *exact parents* of a node X_j across the environments are not known, and they are possibly different. To estimate the coefficients without knowledge of the exact parents, we can consider the set $\widehat{\text{Pre}}(X_j)$, which consists of nodes located before X_j in the topological order $\hat{\pi}$. By regressing X_j on $\widehat{\text{Pre}}(X_j)$ for each environment, we can obtain coefficient estimations, which are the same coefficients obtained by regressing X_j on its exact parents, in large samples.

Theorem 3. *In large samples, let $\{\tilde{\beta}_{jk}^h\}_{k \in \text{Pre}(X_j)}$ be the coefficients obtained by regressing X_j on the feature mapping of $\text{Pre}(X_j)$, and let $\{\beta_{jk}^h\}_{k \in \text{PA}_j}$ be the coefficients obtained by regressing X_j on the feature mapping of PA_j . Then, $\tilde{\beta}_{jk}^h = \beta_{jk}^h$ if $k \in \text{PA}_j^h$, and $\tilde{\beta}_{jk}^h = 0$ if $k \in \text{Pre}(X_j) \setminus \text{PA}_j^h$.*

Proof. Proof can be found in Appendix B.3. \square

Motivated by Theorem 3, and given an estimated $\{\tilde{\beta}_{jk}^h\}_{k \in \widehat{\text{Pre}}(X_j)}$, one could conduct a hypothesis testing as follows:

$$H_0 : \tilde{\beta}_{jk}^1 = \dots = \tilde{\beta}_{jk}^H \quad (13)$$

If the null hypothesis H_0 is rejected, it indicates that there is evidence of a functionally shifted edge between nodes X_k and X_j across the environments. In this paper we leave the hypothesis test unspecified to allow for any procedure that can test eq.(13).

Algorithm 5 Functionally shifted edges detection

Input: Sample data $\mathbf{X}^1, \dots, \mathbf{X}^H$, shifted nodes set \widehat{S} , topological order $\hat{\pi}$, significance level α .

Output: Set of functionally shifted edges \widehat{E}

- 1: **for** $j \in \widehat{S}$ **do**
 - 2: Estimate $\tilde{\beta}_{jk}^h$ for all $k \in \widehat{\text{Pre}}(X_j)$ and $h \in [H]$
 - 3: **for** $k \in \widehat{\text{Pre}}(X_j)$ **do**
 - 4: Conduct hypothesis testing H_0 (equation 13) under significant level α .
 - 5: If H_0 is rejected, add edge $(X_k \rightarrow X_j)$ to \widehat{E} .
-